JCI The Journal of Clinical Investigation

PIK3Cδ expression by fibroblasts promotes triple-negative breast cancer progression

Teresa Gagliano, … , Justin Stebbing, Georgios Giamas

J Clin Invest. 2020. https://doi.org/10.1172/JCI128313.

Research In-Press Preview Cell biology Oncology

Graphical abstract

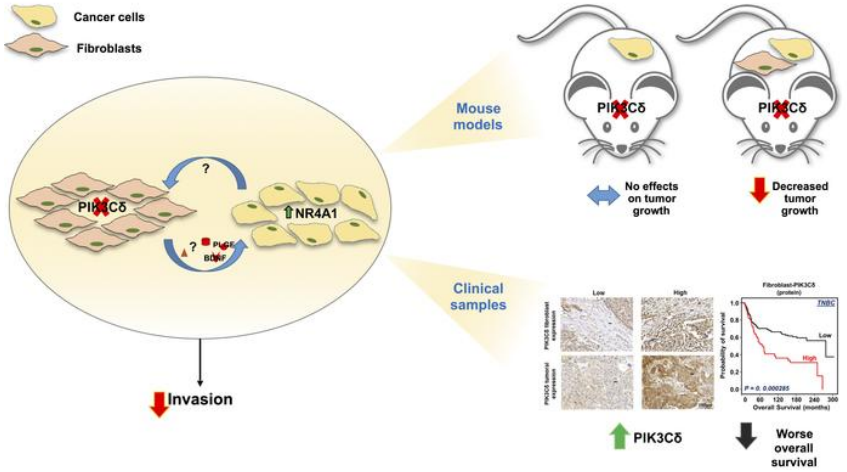

PIK3Cδ expression by fibroblasts promotes triple-negative breast cancer progression

Teresa Gagliano[1,*], Kalpit Shah[2,3,#], Sofia Gargani[4,#], Liyan Lao[5], Mansour Alsaleem[6], Jianing Chen[5], Vasileios Ntafis[4], Penghan Huang[5], Angeliki Ditsiou[1], Viviana Vella[1], Kritika Yadav[7], Kamila Bienkowska[1], Giulia Bresciani[1,8], Kai Kang[9], Leping Li[9], Philip Carter[10], Graeme Benstead-Hum[11], Timothy O'Hanlon[12], Michael Dean[2], Frances M.G. Pearl[11], Soo-Chin Lee[7,13,14], Emad A Rakha[6], Andrew R Green[6], Dimitris L. Kontoyiannis[4,15], Erwei Song[5], Justin Stebbing[10] and Georgios Giamas[1,*]

[1] Department of Biochemistry and Biomedicine, School of Life Sciences, University of Sussex, Falmer, Brighton BN1 9QG, UK

[2] Division of Cancer Epidemiology and Genetics, National Cancer Institute (NCI), National Institutes of Health (NIH), Bethesda, MD 20892, USA

[3] Present address: Bristol-Myers Squibb Co., Princeton, New Jersey 08543, USA

[4] Division of Immunology, Biomedical Sciences Research Center Alexander Fleming, Vari, Greece

[5] Breast Tumor Center, Sun Yat-Sen Memorial Hospital, Sun Yat-Sen University, Guangzhou 510120, China

[6] Nottingham Breast Cancer Research Centre, Division of Cancer and Stem Cells, School of Medicine, Nottingham City Hospital, University of Nottingham, Hucknall Road, Nottingham, NG5 1PB, UK

[7] Cancer Science Institute, Singapore, National University of Singapore

[8] Department of Medical Sciences, University of Ferrara, Italy

[9] Biostatistics and Computational Biology Branch, National Institute of Environmental Health Sciences, NIH, Durham, NC, 27709, USA.

[10] Department of Surgery and Cancer, Division of Cancer, Imperial College London, Hammersmith Hospital Campus, Du Cane Road, London, W12 ONN, UK

[11] Bioinformatics Group, School of Life Sciences, University of Sussex, Falmer, Brighton BN1 9QJ, UK

[12] Cancer Genomics Research Laboratory, Frederick National Laboratory for Cancer Research, Bethesda, MD 20892, USA

[13] Department of Haematology-Oncology, National University Cancer Institute, Singapore

[14] National University Health System, Singapore

[15] Department of Genetics, Development and Molecular Biology, School of Biology, Aristotle University of Thessaloniki, Thessaloniki, Greece

# These authors contributed equally to this study

Keywords: PIK3Cδ; triple negative breast cancer; secretome, RNA sequencing, CAF, TME

*To whom correspondence should be addressed:

Dr Teresa Gagliano and Prof Georgios Giamas
University of Sussex
School of Life Sciences, JMS Building
Falmer, Brighton BN1 9QG, UK
Email: t.gagliano@sussex.ac.uk; g.giamas@sussex.ac.uk

Abstract

As there is growing evidence for the tumor microenvironment's (TME) role in tumorigenesis, we investigated the role of fibroblast-expressed kinases in triple negative breast cancer (TNBC). Using a high-throughput kinome screen combined with 3D invasion assays, we identified fibroblast-expressed PIK3Cδ (f-PIK3Cδ) as a key regulator of progression. Although PIK3Cδ was expressed in primary fibroblasts derived from TNBC patients, it was undetectable in breast cancer cell lines. Genetic and pharmacologic gain- and loss-of functions experiments verified the contribution of f-PIK3Cδ in TNBC cell invasion. Integrated secretomics and transcriptomics analyses revealed a paracrine mechanism via which f-PIK3Cδ confers its pro-tumorigenic effects. Inhibition of f-PIK3Cδ promoted the secretion of factors, including PLGF and BDNF, which led to upregulation of NR4A1 in TNBC cells where it acts as a tumor suppressor. Inhibition of PIK3Cδ in an orthotopic BC mouse model reduced tumor growth only after inoculation with fibroblasts, indicating a role of f-PIK3Cδ in cancer progression. Similar results were observed in the MMTV-PyMT transgenic BC mouse model, along with a decrease on tumor metastasis emphasizing the potential immune-independent effects of PIK3Cδ inhibition. Finally, analysis of BC patient cohorts and TCGA datasets identified f-PIK3Cδ (protein and mRNA levels) as an independent prognostic factor for overall and disease free survival, highlighting it as a therapeutic target for TNBC.

Introduction

Triple negative breast cancer (TNBC; ER^-, PR^-, $HER2^-$) represents a molecularly diverse and highly heterogeneous subtype of BC (15-20%) with a poor prognosis, high rates of recurrence and metastasis. Treatment largely relies on chemotherapy which remains toxic and often ineffective (1, 2).

Despite mounting evidence for the role of the tumor microenvironment (TME) in affecting surrounding cells and its involvement in metastatic progression, little is known about how stromal cells can influence the behavior of cancer epithelial cells and how they affect their response to target therapy (3-5). Under physiological conditions, the stroma serves as a barrier to epithelial cell transformation, while the interplay between epithelial cells and the microenvironment can maintain epithelial polarity and modulate growth inhibition (6). In BC, gene expression analysis of the tumor stroma has led to identification of clusters that can predict clinical outcome (7). In TNBC patients, infiltration of inflammatory cells or the presence of a stroma with reactive, invasive properties, has been associated with a poor prognosis (8, 9).

Fibroblasts are the most prominent cells in the TME and can induce both beneficial and adverse effects in pre-metastatic progression (4, 10). The important functions of fibroblasts include the deposition of extracellular matrix (ECM), regulation of epithelial differentiation, regulation of inflammation and involvement in cell migration (11, 12). Fibroblast-secreted ECM proteins play a vital role in BC onset and progression (13), while cancer-associated fibroblasts (CAFs) have been shown to promotes resistance to cytotoxic and target therapy by secreting protective factors (14). Further understanding the involvement of stromal cells in TNBC, in particular the elucidation of the cross-talk between fibroblasts and BC cells, might lead to the design of new therapeutic strategies and more effective tailored treatments for TNBC patients.

Finak et al. reported that functional inactivation of PTEN, that leads to phosphoinositide 3-kinase (PI3K) activation, in fibroblasts within the breast TME contributes to cancer development and progression (7). We hypothesized that PI3K activity may be a regulator of the tumor-stroma interactions (15) and inhibition of PI3K signaling in fibroblasts could impede its tumor-promoting activity. PI3Ks phosphorylate inositol lipids and are involved in immune response (16-18). Whereas PIK3Cα (p110α) and PIK3Cβ (p110β) are ubiquitously expressed, PIK3Cδ (p100δ) is predominantly expressed in white blood cells (19). However, an unexpected role of PIK3Cδ in oncogenesis of non-hematopoietic cells was observed in avian fibroblasts

where overexpression of wild-type PIK3Cδ induced oncogenic transformation (20, 21).Another report has demonstrated the involvement of PI3K isoforms (including PIK3Cδ) in the differentiation of human lung fibroblasts into myofibroblasts (22). PIK3Cδ contributes to neutrophil accumulation in inflamed tissue by impeding chemoattractant-directed migration as well as adhesive interactions between neutrophils and cytokine-stimulated endothelium (23). Although hampering PI3Ks' activity in fibroblasts would be expected to inhibit stroma mediated tumor-promoting activity, a direct effect of PI3K inhibitors on these cells has not been tested to date.

Herein, using a high throughput siRNA kinome screening we identify fibroblast-expressed PIK3Cδ as a mediator of TNBC development *in vitro* and *in vivo* and we show the mechanism via which fibroblast PIK3Cδ modulates TNBC progression. Our work reveals a previously uncharacterized yet significant role of fibroblast-expressed PIK3Cδ, which supports the rationale for clinical use of PIK3Cδ inhibitors for the treatment of TNBC.

Results

Cancer associated markers in HMF and MRC5 fibroblast cell lines

The primary aim of this work was to examine how normal fibroblasts (NFs) within the TME affect TNBC progression. This reflects several controversial issues that have been raised about the genomic landscape of CAFs and the identification of specific markers that differentiate CAFs. According to recent evidence (8), CAFs in TNBC should be characterized by the combined expression of fibroblast activated protein (FAP), integrin β1 (ITGβ1/CD29) S100A4, PDGFRβ, α-smooth muscle actin (α-SMA) and Caveolin. Therefore, the expression of CAF markers was evaluated in the fibroblast cell lines used herein (HMF and MRC5) and were also compared to primary fibroblasts (NFs and CAFs) obtained from four TNBC patients (**Supplementary Table 1**). The separation of primary CAFs from NFs was based on the distance from the site of the primary tumor (CAFs<5cm; NFs >5cm).

As shown in **Supplementary Figure 1A**, PDGFRβ was more abundant in CAFs compared to NFs while Caveolin was downregulated in CAFs. Overall expression and changes in FAP levels were related to patient's variability rather than the fibroblast site of origin. ITGβ1 and α-SMA were widely expressed in all samples, while S100A4 was hardly detectable in primary fibroblasts. The expression levels of the CAF markers in HMF and MRC5 were comparable to those in the primary fibroblast cell lines. PDGFRβ, ITGβ1, FAP, Caveolin and α-SMA were equally detected in HMF and MRC5 cells while S100A4 was solely present in HMF.

Although the expression of these markers in HMF and MRC5 were comparable to those found in primary fibroblasts of TNBC tumors, there was no clear distinction between NFs and CAFs based on these proteins, which supports the aforementioned controversy. In contrast, the similarities between HMF/MRC5 and primary fibroblasts in the expression of CAF-markers support the use of these cells as a model to study cancer cells-fibroblasts interactions. Nevertheless, since our goal is not restricted to a specific fibroblast subtype, we used both HMF and MRC5 in our experiments.

High-throughput (HT) RNAi screening identifies fibroblast-expressed kinases involved in TNBC cell invasion

Based on the established role of protein kinases (PKs) as drug targets and considering the fact that intra- and extra-cellular signaling is mainly transmitted through PKs, we investigated the role of fibroblast-expressed kinases on TNBC progression. Hence, we established an

experimental pipeline (**Figure 1A**), broadly applicable to different systems that consisted of a 3D co-culturing model (cancer and stromal cells) linked to an invasion assay as a readout tool.

The primary screening was performed in duplicate in HMF and once in MRC5 cells. Fibroblast cell lines were transfected with a pool of 3 siRNAs/gene targeting each of the 710 human kinases (**Figure 1A**; *Step 1*). 24 hours after transfection, HMF or MRC5 were co-cultured in 3D with MDA-MB-231 and after 3 days, required for spheroids formation, Matrigel and chemoattractants were added to the wells to promote invasion (**Figure 1A, Supplementary Figure 2 and Supplementary Videos 1 & 2**; *Step 2*). Pictures of spheroids taken after 3 and 6 days were analyzed and the results were expressed as changes in spheroid surface (Δ= $Surface_{Day6}$ - $Surface_{Day3}$). The Δ-value of each silenced kinase (Δ_K) was compared with the Δ-value of the control (Δ_{CT}), at different time-points, to obtain a Δ_{Ratio} ($\Delta_{Ratio}= \Delta_{CT}/\Delta_K$) (**Figure 1A**; *Step 3*). Kinases were divided depending on their effects on MDA-MB-231 invasion and those with a ΔRatio ≤ 0.5 (50% less invasion vs CT) and $p<0.01$ (as well as SD < 0.5 for HMF), were considered as 'invasion-promoting', while kinases with a ΔRatio > 2 (100% more invasion vs CT), $P > 0.05$ (as well as SD > 0.5 for HMF) were considered as 'invasion inhibiting' ones. The Δ_{Ratio} values were used to calculate the Z-Scores and all hits were plotted for both cell lines, revealing new potential fibroblast-expressed kinases able to modulate TNBC cell invasion (**Figure 1B and Supplementary Figure 3**; *Step 4*). All screening data are presented in **Supplementary Table 2**.

Based on pre-specified cut-off criteria, we identified 17 kinases in HMF and 64 in MRC5 whose silencing decreased the rate of TNBC invasion (~40%-90%), suggesting a pro-invasive role of these proteins (**Figure 2A**). Under these conditions, there were two shared targets amongst HMF and MRC5: PIK3Cδ and AURKA. Using a panel of fibroblasts and breast cancer (BC) cells, we analyzed the levels of PIK3Cδ and AURKA and discovered a variability in their expression amongst the primary and immortalized fibroblast cell lines (**Figure 2B, Supplementary Figure 1B**). PIK3Cδ protein levels in fibroblast cells were comparable to those in the BJAB B-cell line (used as a positive control) (24) while intriguingly PIK3Cδ was hardly detectable/totally absent in most of the BC cells, as opposed to AURKA, which was ubiquitously expressed (**Figure 2C, Supplementary Figure 1C and Supplementary Figure 4D-*upper panel***). qRT-PCR analysis of PIK3Cδ revealed a similar trend for most of the cell lines tested (**Supplementary Figure 4A**), though it is well-known that protein and mRNA abundances do not always correlate (25, 26). Moreover, RNA sequencing (RNAseq) in different organs obtained from the Human Protein Atlas (27) revealed that apart from myeloid

and lymphoid cells, fibroblast cell lines express moderate/high PIK3Cδ mRNA levels in contrast to BC cell lines that have low/negligible mRNA transcripts (**Supplementary Figure 4B**). We also investigated whether fibroblast-PIK3Cδ can induce the expression of PIK3Cδ in TNBC following extended co-culturing between the different cell types. As shown in **Supplementary Figures 4C and 4D**, by using both fibroblast cell lines and primary CAFs derived from MMTV-PyMT tumors, there were no changes of PIK3Cδ in TNBC cells, maintaining their low/undetectable protein levels.

Altogether, these results suggest that PIK3Cδ could not have been identified if we were solely studying BC cells instead of examining their interactions with the surrounding stroma, further supporting the setup of our experimental approach by regarding cancer as a systemic multi-cell lineage dependent disease. We further validated the involvement of fibroblast PIK3Cδ-mediated TNBC 3D invasion by repeating the experiment following silencing (**Figure 2D**) or overexpression of (**Figure 1G**) PIK3Cδ. Similar data were obtained using MDA-MB-231, BT-549 and fibroblast cell lines (**Supplementary Figures 5A-5F**). Finally, we determined that treatment of TNBC cells with conditioned media (CM) derived from genetically modified fibroblasts (PIK3Cδ-silenced or PIK3Cδ-overexpressed) has no significant effect on TNBC cell proliferation (**Supplementary Figure 5G**). Taking everything into consideration and bearing in mind the potential implication in BC we focused on PIK3Cδ and investigated its fibroblast involvement.

Confirmation of HT-RNAi screening results

The accuracy and validity of our experimental pipeline/screening was supported by identification of kinases (positive hits) whose involvement in stromal-mediated cancer invasion has been previously reported. Amongst these results were FLT4 (28) and EGFR (29) (invasion-promoting) as well as ACVR1B (30) and ITPKB (31) (invasion-inhibiting).

To further validate the of HT-RNAi screenings results, we performed the experimental pipeline by using shRNA plasmids targeting randomly selected kinases. As shown in **Supplementary Figure 6A**, the effects of shRNA-mediated silencing of the tested kinases in MRC5 led to similar effects on the invasion of MDA-MB-231 as observed in the primary screening. The gene knockdown efficiency was confirmed by real-time qRT-PCR (**Supplementary Figure 6B**).

Next, we examined the effects of 8 specific inhibitors against the randomly selected and shRNA-validated kinases that affected invasion in the MRC5 screening and repeated the

experiment. As anticipated, similar results were observed, although in some cases (i.e. AZD4547) the results were not identical to the primary screening (**Supplementary Figures 6C**). This could be due: (i) to potential off-target effects of some inhibitors, (ii) to the fact that some inhibitors can target other isoforms of a specific kinase and/or (iii) because the genomic vs the chemical/pharmacological inhibition of a kinase does not necessarily have the same outcome.

Regarding the overlapping hits from our screening (PIK3Cδ and AURKA), we verified that the observed effects on MDA-MB-231 cell invasion, following genomic inhibition (siRNA), is not based on a reduction (**Supplementary Figure 6D**) or an increase (PIK3Cδ overexpression; **Supplementary Figure 6E**) of cell viability.

Genomic or chemical inhibition of PIK3Cδ in fibroblasts reduces TNBC cell invasion as a result of paracrine signaling

To clarify whether the catalytic activity of PIK3Cδ is required for its effect on TNBC progression, we repeated our 3D spheroid invasion assay following chemical inhibition of PIK3Cδ in fibroblast cells, using CAL-101 (Idelalisib; a highly selective and potent PIK3Cδ inhibitor) (32). HMF or MRC5 were initially treated with different concentrations of CAL-101 for 24h, while the efficacy of CAL-101 inhibition on downstream targets of PIK3Cδ was validated (**Supplementary Figure 7A**). Moreover, treatment with CAL-101 had limited/no effects on fibroblasts' cell viability for the 24h period of treatment (**Supplementary Figure 7B**). Nevertheless, to avoid any misinterpretations, fibroblasts were washed with PBS, counted with trypan blue and only viable cells were used in co-cultures with TNBC cells (MDA-MB-231 or BT-549) at a 1:1 ratio. CAL-101 pre-treated fibroblasts showed a decrease in 3D-spheroid invasion (**Figure 3A and Supplementary Figure 8A**), suggesting that the kinase activity of PIK3Cδ is, to a great extent, responsible for the observed results.

Intercellular communication sets the pace for transformed cells to survive and to thrive. Based on the initial setup of our assay (3D-spheroids/cells co-culture), we could not be certain whether the involvement of stromal PIK3Cδ on TNBC progression is a result of juxtacrine signaling (cell-to-cell contact-dependent) or a consequence of paracrine signaling due to secreted factors derived from fibroblasts that can alter the behavior of TNBC cells. Hence, we implemented a transwell assay, where HMF or MRC5 cells pre-treated with CAL-101, were seeded on the lower chamber of the inserts and 24h later co-cultured with TNBC cells platted on a Matrigel-coated top chamber to assess the 2D invasion potential of TNBC cells (**Figure**

3B and Supplementary Figure 8B). Using a similar experimental principle, we employed the xCELLigence Real-Time Cell Analysis (RTCA) instrument (33), to monitor the real-time invasion rate of TNBC cells following co-culturing with fibroblasts pre-treated with CAL-101 (**Figure 3C and Supplementary Figure 8C**). Both assays revealed a reduction in invasiveness after inhibition of fibroblast-PIK3Cδ activity. Similar results were observed when we implemented another method for indirect contact co-cultures using the CM of CAL-101 treated HMF or MRC5 and examining their effects on TNBC invasion (**Figure 3D and Supplementary Figure 8D**). Moreover, 2D invasion assays of either MDA-MB-231 or BT-549 cells co-cultured with primary TNBC CAFs showed comparable results further highlighting the role of fibroblast-PIK3Cδ (**Supplementary Figure 9**).

To further demonstrate the contribution of PIK3Cδ in the observed phenotype and rule out any off-target effects, we repeated the 2D invasion assays by silencing PIK3Cδ and then performed a recovery experiment by re-introducing/overexpressing PIK3Cδ. As expected, by recovering PIK3Cδ levels (**Supplementary Figure 10A**), we reversed the decrease in invasion that was induced by genetic inhibition of PIK3Cδ (**Supplementary Figure 10B**).

Next, to examine the possibility of other fibroblast-expressed PI3K isoforms contributing to the decrease of TNBC cell invasion, in particular PI3KCγ that can also be inhibited by CAL-101, we repeated the 2D invasion assays using various PI3K inhibitors (**Supplementary Figure 11A**). Treatment with AS252424 (PIK3Cγ/α inhibitor) had minor effects on TNBC cell invasion, as compared to either CAL-101 or Leniolisib (PIK3Cδ inhibitor). Furthermore, use of the pan-PIK3C inhibitors, PI-103 and NVP-BEZ235 had analogous effects with the PIK3Cδ inhibitors, further supporting the importance of PIK3Cδ in the observed phenotype (**Supplementary Figure 11B**). Finally, we verified that the observed effects on MDA-MB-231 cell invasion, following treatment with the different PIK3 inhibitors, is not based on a reduction of cell viability (**Supplementary Figure 11C**).

Taken together all combinations of cell lines and assays used, our results demonstrated that fibroblast-PIK3Cδ promotes TNBC progression via paracrine regulatory mechanisms.

Integrated secretome/transcriptomic analyses reveal fibroblast PIK3Cδ-mediated paracrine mechanisms that promote TNBC progression

We and others (34, 35) have shown that co-culture of stromal with BC cells leads to changes in protein expression supporting the hypothesis of cross-talk between different cell types. Changes of PIK3Cδ activity in fibroblasts can alter the intercellular communication between

stromal and cancer cells thereby affecting their biological properties. To gain insights into the paracrine mechanisms employed by fibroblasts to promote invasion in TNBC cells, we performed an integrated analysis of proteins secreted by HMF and MRC5 treated with CAL-101 and the transcriptome of MDA-MB-231 cells which were grown in a transwell setup with CAL-101 treated MRC5 cells.

Based on our 2D/3D co-culture results, we analyzed the PIK3Cδ-regulated secretome, using the Human L1000 Array. HMF and MRC5 cells were treated with either DMSO or 10 μM CAL-101 for 24h and cell culture supernatants were isolated and processed according to the manufacturer's instructions. By employing differential expression analysis, we identified a total of 206 and 377 secreted proteins that were significantly regulated by CAL-101 treatment of HMF and MRC5 respectively at the Log2 fold difference of |0.5| and a P-value of ≤ 0.05. We found that 73 secreted proteins were common between CAL-101 treated HMF and MRC5 cells, providing evidence for a mechanism of fibroblast-mediated regulation of TNBC aggressiveness (**Figure 4A, Supplementary Table 3**). To gain additional insights into the similarities and differences in CAL-101 mediated effects on the secretome, we generated an upset plot of differentially expressed secreted proteins from CAL-101 treated HMF and MRC5 cells. As shown in **Figures 4B and 4C,** CAL-101 upregulated a common set of 40 proteins and downregulated a set of 5 proteins in both HMF and MRC5 cells, while 28 proteins were differentially regulated by CAL-101 in HMF and MRC5.

With comprehensive profiling of CAL-101 mediated changes in the secretome of fibroblast cell lines established, next we investigated how these secreted proteins altered the transcriptional state of MDA-MB-231 cells. We cultured MDA-MB-231 in a transwell along with CAL-101 or vehicle-treated MRC5 cells for 24 hours and total RNA was extracted from MDA-MB-231 and processed as described before (36). Whole transcriptome data showed a high degree of similarity between replicate samples and most significant variations between MDA-MB-231 cells co-cultured with CAL-101 treated or untreated MRC5 cells (**Supplementary Figure 12**). The principal component analysis (PCA) support our hypothesis that inhibition of PIK3Cδ in fibroblasts has a paracrine effect on TNBC cells.

We next employed differential gene expression analysis using the DESeq2 pipeline to identify genes dysregulated in MDA-MB-231 cells as a consequence of inhibiting PIK3Cδ in MRC5 cells. We found 137 genes here at the false discovery rate Padj ≤ 0.05 (**Figure 4D and Supplementary Table 4**). Only 24/137 genes, were significantly dysregulated at the false discovery rate Padj ≤ 0.05 and Log2 fold difference of ≥ |0.5| (**Figure 4E**). We validated the

RNASeq analysis using an orthogonal approach of real-time qRT-PCR in independent experiments using a separate cohort including the effects of overexpression of PIK3Cδ on NR4A1 mRNA levels (**Figure 4F, and Supplementary Table 5**). Amongst the most significantly modulated genes was NR4A1 transcription factor, which was recently reported to be implicated in TNBC invasion (37). The increase on NR4A1 protein levels in MDA-MB-231 cells following co-culture with CAL-101 treated MRC5 cells was also confirmed (**Figure 4G**).

Overall, these results show that pharmacological inhibition of PIK3Cδ in fibroblast cells not only alters its secretome, but also has a subtle paracrine effect on the gene expression of cancer cells.

Promotion of TNBC invasion via the fibroblast/epithelial-mediated PIK3Cδ-PLGF/BDNF-NR4A1 signaling pathway

Following confirmation of NR4A1 protein expression in different BC cell lines (**Supplementary Figure 13A**) and to further demonstrate its involvement in TNBC, we treated cells with cytosporone B, an agonist of NR4A1 (38) and examined its effects on the invasiveness of MDA-MB-231 and BT-549 cells. As expected, cytosporone B significantly decreased the invasiveness of TNBC cells (**Figure 5A and Supplementary Figure 13B**). On the contrary, silencing of NR4A1 increased the invasive ability of MDA-MB-231 cells (**Figure 5B**). Moreover, in the NR4A1-silenced cells, the effects of cytosporone B was almost completely abrogated (**Supplementary Figure 13G**). Silencing of NR4A1 was confirmed by qRT-PCR and western blotting (**Supplementary Figures 13D and 13E**) and in order to exclude possible off-targets effects, NR4A2 and NR4A3 mRNA levels were analyzed by qRT-PCR in NR4A1 silenced cells (**Supplementary Figures 13F**).

Additionally, we investigated the effects of PIK3Cδ overexpression in MRC5 cells on the invasiveness of MDA-MB-231 cells pre-treated with cytosporone B in order to increase their NR4A1 levels. As shown in **Figure 5C**, PIK3Cδ partly rescued the inhibitory effects of NR4A1 activation, demonstrating the PIK3Cδ-NR4A1 paracrine signaling axis between fibroblast and TNBC epithelial cells. To examine if the effects of PIK3Cδ inhibition (CAL-101) on TNBC cell invasion are related to NR4A1 expression, we performed a 2D-invasion assay in which MRC5 (or HMF) were treated with CAL-101 (or DMSO), while NR4A1 was silenced in MDA-MB-231 cells. As shown in **Figure 5D and Supplementary Figure 13C**, silencing of NR4A1 completely abrogated the effects of CAL-101 on TNBC cell invasion. Moreover, the NR4A1 silencing-mediated induction of invasion was abolished when fibroblasts were pre-treated with CAL-101 (**Figure 5D**), which is due to the paracrine induction of NR4A1 expression caused

by CAL-101 (**Figure 3F**) that balances the NR4A1 siRNA knock-down. Indeed, when NR4A1-silenced cancer cells were co-cultured with CAL-101 treated-fibroblasts, NR4A1 levels were restored (comparable to those of the control), thus siNR4A1 MDA-MB-231 cells co-cultured with CAL-101 treated MRC5 cells completely restore the baseline conditions in terms of NR4A1 levels as well as the invasion levels compared to those of MDA-MB-231 co-cultured with MRC5 cells (**Figure 5D**; right panel). Together, these results suggest the existence of a direct association between fibroblast PIK3Cδ-mediated reduction of invasion and TNBC cells' NR4A1 levels.

Having built a comprehensive dataset of secreted proteins from CAL-101 treated MRC5 cells and the transcriptome of MDA-MB-231 co-cultured with CAL-101 treated MRC5 cells, we performed an integrated transcriptomics-proteomics analysis to unravel mechanisms employed by stromal cells to promote invasion in malignant cells.

We hypothesized that secreted factors derived from CAL-101 treated MRC5 and HMF cells may alter cell-cell communication pathways and regulate the invasion of MDA-MB-231 cells by modulating the expression of invasion related genes including *NR4A1*, which was shown to be overexpressed in our transcriptomic analysis (**Supplementary Table 4**). To test this hypothesis, we employed the Ingenuity Pathway Analysis (IPA) software and literature mining to curate a list of potential PIK3Cδ-regulated secreted proteins that are enriched in cell migration/invasion pathways and are also known to modulate NR4A1expression. Our analytical method, which is described in **Supplementary Figure 14**, identified several secreted factors (n=40) that were directly involved in pathways regulating cellular movement or cell-to-cell signaling mechanisms **(Supplementary Table 6**), amongst which certain of them have been reported to have an association with *NR4A1* expression, including placental growth factor (PLGF) (39, 40) and brain-derived neurotrophic factor (BDNF) (41) (**Supplementary Figure 15**). Scatter plots displaying all secreted proteins from CAL-101 treated MRC5 and HMF while highlighting the list of potential candidates regulating NR4A1 expression in MDA-MB-231 are shown in **Figures 6A and 6B**.

Previous studies have demonstrated that induction of NR4A1 by PLGF inhibits endothelial cell proliferation (42, 43), while PLGF can also impede tumor growth and metastasis (44). Moreover, BDNF has been described to have a role in BC progression (45), even though its exact role has not been completely clarified. Treatment of MDA-MB-231 or BT-549 cells with PLGF or BDNF confirmed its positive effects on NR4A1 supporting their contribution in the paracrine upregulation of NR4A1 mRNA/protein levels (**Figures 6C, 6D and Supplementary**

Figure 16A). Moreover, PLGF and BDNF also led to a significant decrease in TNBC invasion (**Figure 6E and Supplementary Figure 16B**). Finally, we confirmed that silencing of either BDNF or PLGF in fibroblasts attenuated the CAL-101-mediated reduction of TNBC cell invasion, further supporting the involvement of this pathway, while suggesting the existence of additional mechanisms implicated in the described phenotype (**Supplementary Figure 17A**). Interestingly, silencing of BDNF and/or PLGF did not affect TNBC invasion, suggesting that the PIK3Cδ effects are exerted during membrane trafficking and/or secretion of these factors and not at the gene/protein expression level. This is in accordance with previous reports describing a role of CAL-101 in down-regulating secretion, rather than expression, of chemokines in stromal co-cultures (32). In addition, silencing of BDNF and/or PLGF abolished the CAL-101 inhibitory effects on fibroblast-mediated invasion, without affecting basal invasion levels. This may be due to the experimental design, since silencing of a gene does not have an immediate effect on the respective total and/or secreted protein levels. Finally, it is worth mentioning that other mechanisms/factors could also contribute to the fibroblast-mediated invasion. Silencing of BDNF and PLGF was confirmed by qRT-PCR (**Supplementary Figure 17B**).

In summary, our results reveal a novel paracrine signal transduction pathway between fibroblasts and TNBC cells, encompassing PIK3Cδ-PLGF/BDNF-NR4A1 (**Figure 6F**), without ruling out the existence of other mechanisms contributing to the observed phenotype.

Pharmacological inhibition of fibroblast PIK3Cδ reduces BC tumor growth *in vivo*

Next, we used an orthotopic BC xenograft model where MDA-MB-231 or MDA-MB-231 with MRC5 were co-injected in the mammary fat pads of NOD SCID mice in order to examine the effects of PIK3Cδ inhibition. After tumor formation and mice randomization, perioral (PO) administration of CAL-101 or vehicle (30% PEG 400 +0.5% Tween 80) was initiated for both groups according to the scheme in **Figure 7A**.

As previously reported (46), cancer cells in the co-injected tumors (MDA-MB-231+MRC5) exhibited larger tumor volumes (**Figure 7B**) and a higher proliferative rate (Ki-67 labelling, **Figure 5C**). Moreover, CAL-101 treatment of MDA-MB-231 tumors did not significantly affect their *in vivo* growth (**Figure 7B**), in agreement with our cell-based data that demonstrated only a marginal inhibitory effect of CAL-101 on MDA-MB-231 proliferation (**Supplementary Figure 18**). Interestingly, MDA-MB-231+MRC5 tumors were reduced following treatment with CAL-101 (**Figure 7B**; Day 14: 48.28% average reduction; Day 21: 23.65% average reduction). The efficacy of CAL-101 on PIK3Cδ activity was validated by assessing the

expression of pAKT via immunohistochemistry on tissue samples (**Figure 7D**). Moreover, the presence of human fibroblasts in MDA-MB-231+MRC5 tumors was confirmed in cryosection slides using a human anti-fibroblast antibody (**Figure 7E**). We also checked for $CD68^+$ (monocytes / macrophages) cells, however we only detected a small population of these tumor infiltrating cells, which is consistent with the immunocompromised background of this mouse strain (**Supplementary Figure 19**). Finally, animals treated with CAL-101 did not display any significant changes in weight nor gross phenotypic changes, indicating that that the treatment did not cause any adverse or toxic effects.

As a proof of concept of the potential use of PIK3Cδ inhibitors for BC treatment, we employed the MMTV-PyMT transgenic model (47). MMTV-PyMT mice received daily oral administration of either control vehicle or CAL-101 (10 mg/kg) for a period of six weeks. Our results revealed a significant reduction in tumor growth following CAL-101 treatment (**Figures 8A, 8B and Supplementary Figures 20A, 20B**). Moreover, the number of lung metastasis nodules was significantly reduced in the CAL-101 group, compared with the control group, as evidenced by H&E staining and macroscopic observation of lung specimens (**Figure 8C and Supplementary Figures 20B and 20C**). Furthermore, following CAL-101 treatment, the expression of p-AKT was decreased in tumor infiltrating fibroblasts (a-SMA^+) (**Figures 8D**), besides from macrophages ($F4/80^+$) (**Figure 8E**), while no changes were observed in the total PIK3Cδ levels of fibroblasts or macrophages (**Supplementary Figures 20D and 20E**). In addition, as demonstrated in TNBC and fibroblast cell lines (**Supplementary Figure 4C**), PIK3Cδ was exclusively expressed in CAFs isolated from MMTV-PyMT tumors, while cancer cells had low/undetectable levels of PIK3Cδ, the expression of which did not change following co-culturing with CM isolated from CAFs (**Supplementary Figure 20F**), further supporting the *in vitro* evidence that the effects of CAL-101 are cancer cells-independent. Finally, IHC analysis of MMTV tumors revealed an increased expression of NR4A1 along with PLGF and BDNF following CAL-101 treatment (**Supplementary Figure 21**) supporting our cell-based data.

Taken together, these results highlight the involvement of fibroblast-expressed PIK3Cδ in promoting BC growth *in vivo*.

High fibroblast PIK3Cδ expression correlates with poor patient outcome in TNBC

Finally, we investigated the plausible role of fibroblast (a-SMA^+) or tumor-expressed (cancer cells) PIK3Cδ in a clinical setting by analyzing a well-characterized TNBC patients' cohort (n=179) (48, 49). The clinico-pathologic parameters are summarized in **Supplementary Table**

7. PIK3Cδ expression was variable in both tumor (H-score range 20-220) and surrounding cancer associated fibroblasts (5-100%) with high PIK3Cδ tumoral expression (H-Score >130 observed in 31/179 cases (17%) whereas fibroblasts showed high PIK3Cδ (>85%) in 44/179 (25%) of the cases (**Figure 9A and Supplementary Figure 22**).

Analysis of the surrounding stromal (a-SMA$^+$) PIK3Cδ expression, revealed PIK3Cδ as an independent prognostic factor for overall survival (OS; P = 0.000285; **Figures 9B**) and disease free survival (DFS; P = 0.048; **Figure 9C**), indicative of fibroblast-PIK3Cδ's involvement in TNBC progression. Multivariate analyses demonstrated that PIK3Cδ in the surrounding cancer fibroblasts was also an independent prognostic factor for OS (P = 0.001), DFS (P = 0.044), age and nodal stage (**Supplementary Table 8**). Similar analyses revealed that, high PIK3Cδ protein levels in tumoral-PIK3Cδ were associated with a significantly shorter OS (P = 0.0004) and DFS (P = 0.009) (**Supplementary Figures 23A and 23B**), while tumoral-PIK3Cδ was an independent prognostic factor of age, nodal stage and lymphovascular invasion (LVI) status and for predicting OS (P = 0.006) and DFS (P = 0.028) (**Supplementary Table 9**). Interestingly, investigation of fibroblast-PIK3Cδ in an ERα$^+$ patients' cohort from Singapore (n=73; P = 0.703) did not reveal any correlation with survival outcome (**Figure 9D and Supplementary Tables 10-12**).

We also employed another approach to investigate the potential association of CAF-PIK3Cδ mRNA levels with survival outcomes of ERα$^+$, HER2$^+$ and TNBC subtypes, by de-convoluting bulk RNA-seq samples from TCGA BC data. As illustrated in **Figure 9E**, TNBC patients (n=108) with high CAF-expressed PIK3Cδ levels had shorter OS compared to those with low CAF-expressed PIK3Cδ (P = 0.001), in agreement with our IHC data. Conversely, when studying the bulk tumors, there was no significant association between PIK3Cδ mRNA levels and TNBC patients' survival outcome (P = 0.405; **Supplementary Figure 23C**), opposite to the IHC data, emphasizing the discrepancies that can arise when examining mRNA vs protein levels, which can lead to different conclusions. In addition, these results also highlight the importance of comprehensively analyzing the different cell types separately within the TME. Moreover, expression of CAF-PIK3Cδ mRNA levels were not predictive for survival neither for ERα$^+$ (n=778, P = 0.0584; **Figures 9F**) -recapitulating the IHC data- nor for HER2$^+$ (n=160, P = 0.684; **Figures 9G**) BC subtypes, further underlining the significance of fibroblast-expressed PIK3Cδ isoform in TNBC specifically.

We analyzed the association between the mRNA expression levels of CAF-PIK3Cα, -β, and -γ isoforms and patients' survival for all BC subtypes. Our results revealed that in TNBC high

CAF-expressed PIK3Cα (P = 0.01; **Supplementary Figures 23D**) or CAF-expressed PIK3Cβ (P = 0.01; **Supplementary Figures 23E**) were correlated with shorter OS, while there was no association of either PIK3Cα or PIK3Cβ with ERα^{+} or HER2^{+} BC patients' survival (ERα^{+} patients: PIK3Cα, P = 0.106 ; PIK3Cβ, P = 0.15. / HER2^{+} patients: PIK3Cα, P = 0.731; PIK3Cβ, P = 0.849). Regarding CAF-PIK3Cγ mRNA levels, there was no correlation with survival in neither TNBC (**Supplementary Figures 23F**) nor any of the other BC subtypes (ERα^{+} patients: PIK3Cγ, P = 0.137. / HER2^{+} patients: PIK3Cγ, P = 0.943).

In conclusion, our results demonstrate the clinical significance of fibroblasts-expressed PIK3Cδ in TNBC.

Discussion

TNBC represents an aggressive BC subtype where there remains an unmet clinical need; currently the recommended therapeutic approach in the neoadjuvant, adjuvant and metastatic settings are based on chemotherapeutics (most often platinum-, anthracycline or taxane -based) with recent data suggesting roles for antibody-drug conjugates and immunotherapies (50-53). However, fewer than 30% of women with metastatic TNBC will survive 5 years after diagnosis (54). Sequencing and other 'omics' have revealed an unexpected level of heterogeneity in TNBCs and led to identification of potential actionable targets (52).

However, translational research and clinical trials usually focus on targeting epithelial cancer cells. This is likely to diminish the contribution of reciprocal interactions between malignant and stromal cells that creates a local microenvironment, which fosters tumor growth and also influences responses to treatment (55). The prognostic and predictive significance of gene/protein expression signatures of the surrounding stroma have been well-documented and could represent unexplored ground within the TME which could then be used to improve therapies and outcomes.

PKs are involved in every aspect of cell activity and perturbation of their signaling can contribute to human diseases including malignancies (56-59). Pharmaceutical intervention targeting aberrant kinase signaling represents the major therapeutic approach but although targeted therapies against PKs have improved the clinical outcome of patients, resistance to these treatments develops (60), emphasizing the need for the identification of new druggable targets.

Despite extensive research describing deregulated kinase activity in cancer cells, there has been no thorough and comprehensive investigation about how kinases expressed in stromal cells can influence tumor growth and malignant progression. Therefore, we focused on fibroblasts, the main stromal component in the TME, whose multiplex role in BC initiation, progression and therapy-resistance has been well described (7, 13, 14). We performed a kinome siRNA screening in two different fibroblast cell lines, aiming to identify kinases responsible for stroma-tumor cross-talk. Our siRNA screening/3D co-culturing model was linked to an invasion readout assay that could be performed easier and more reliably by using TNBC cell lines, considering their invasive potential, compared to the non-invasive and less aggressive ER^+ luminal BC cells. However, our findings do not rule out the possibility that these targets can also be linked to other BC subtypes. Ultimately this study aimed to identify targets that are associated with an aggressive phenotype, invasion being the clearest readout. Nevertheless, the

original screening is not designed to identify a mechanism of action and therefore the target's effects could be diverse once studied further (e.g. *in vivo*).

Considering the limited available therapeutic options for TNBC, we focused on this subtype since the identification of new putative druggable targets for TNBC is fundamental. Amongst a subset of differently fibroblast-expressed kinases that could modulate TNBC progression, PIK3Cδ was one of the prominent hits. Despite the involvement of PI3K activity in tumor-stroma interactions (15), still the possibility of using PI3K inhibitors on fibroblasts has not been considered to date.

Given its almost exclusive expression in fibroblasts, PIK3Cδ could not have been identified by focusing solely on TNBC cells, further supporting that the contribution of the TME in cancer development and progression needs to be studied in detail. Using 2D and 3D co-culturing models we determined that fibroblast-expressed PIK3Cδ is integral in TNBC progression. We validated our findings using genomic approaches (loss and gain of function experiments) and we assessed the effects of the chemical inhibition of PIK3Cδ, using a highly selective FDA approved PIK3Cδ inhibitor (CAL-101/Idelalisib) (61), confirming that the catalytic activity of fibroblast PIK3Cδ is required for its paracrine effects on TNBC cells. Mechanistically, using an integrated analysis of the fibroblast PIK3Cδ-regulated secretome and its paracrine mediated transcriptomic changes in TNBC cells, we identified secreted factors and genes that represent key signaling pathways contributing towards the observed PIK3Cδ-induced tumor promoting phenotype. We focused on the link between the overexpression of fibroblast-secreted factors, including PLGF and BDNF, and the upregulation of NR4A1 transcription factor in TNBC epithelial cells, after inhibition of fibroblast-PIK3Cδ. NR4As nuclear receptors are involved in metabolic, cardiovascular and neurological functions, as well as in inflammation and cancer (62-65). Despite the structural similarities of NR4A1, NR4A2 and NR4A3 they display distinctive roles and specific functions (66). Intriguingly, NR4A1 has been reported to act as a tumor suppressor implicated in TNBC proliferation, viability, migration and invasion (37). Our results support a model where inhibition of fibroblast-expressed PIK3Cδ impedes TNBC progression, by promoting the secretion of PLGF, BDNF and other factors, which in turn lead to the paracrine upregulation of NR4A1 in TNBC cells (**Figure 4I**). The existence of additional direct and/or reciprocal signaling pathways originated from cancer cells towards fibroblasts, which could potentially affect PIK3Cδ expression and ultimately contribute to this phenotype, merits further investigation.

To examine the effects of fibroblast-expressed PIK3Cδ on TNBC growth *in vivo*, we initially attempted to generate stable PIK3Cδ knock-out (KO) HMF and MRC5 cell lines and compare their involvement in tumor growth vs PIK3Cδ wild-type fibroblasts. However, PIK3Cδ-KO clones exhibited a relative slow growing rate and considering also the fact that fibroblasts can easily differentiate (67), led us to the alternative option of pharmacologically (CAL-101) inhibiting PIK3Cδ. CAL-101 had no effect when used as a treatment on MDA-MB-231 tumor growth, similarly to what we observed in our cell-based proliferation data when MDA-MB-231 cells were directly treated with CAL-101. Moreover, CAL-101 was administered orally in immune-deficient mice which, combined with the lack of any MDA-MB-231 tumor inhibition, suggests that there were systemic responses initiated from other sub-populations of cells within the TME. This result, along with a recent report, where the authors showed that pharmacological inhibition of PIK3Cδ impedes *in vivo* tumor growth by targeting cancer cells and macrophages, further supports the stromal involvement of PIK3Cδ in BC and the potential use of PIK3Cδ inhibitors in a clinical setting.

In our immunocompromised xenograft model, we initially verified that the co-injection of fibroblasts (MDA-MB-231+MRC5) had an additive effect in tumor formation, when compared to MDA-MB-231 cancer cells alone. More importantly, we observed a decrease in MDA-MB-231+MRC5 tumors following daily treatment with CAL-101. Considering that the only variable between the two mouse models was the introduction of fibroblasts, it is clear that the anti-tumor effects of CAL-101 were conferred via their actions on fibroblasts. Noteworthy, the tumor growth reduction that was observed on Day 21 between MDA-MB-231+MRC5 CAL-101-treated tumors vs MDA-MB-231+MRC5 vehicle-treated ones was borderline non-significant despite the 23.65% median reduction (it is worth mentioning that alternative statistical tests gave a significant P value). We attributed this to the progressive population dilution and decreased viability of human fibroblast cells (MRC5) as the tumor size increases, causing a reduction in relative potency of CAL-101 (as the dosage was left unchanged) on fibroblast PIK3Cδ and its paracrine consequences. Moreover, our results in MMTV-PyMT transgenic mice revealed a significant reduction in primary tumor growth and in metastasis following treatment with CAL-101. The downregulation of PIK3Cδ's activity in fibroblasts, apart from macrophages, implies of a prospective additive, immune-independent mechanism of action of PIK3Cδ inhibitors for cancer treatment. In addition, as fibroblasts have been reported to influence a number of other immune cells, namely monocytes and macrophages

(68, 69), the existence of additional PIK3Cδ-mediated paracrine signaling effects between different cell types could not be ruled out.

The translational significance of fibroblast-expressed PIK3Cδ was validated in a TNBC cohort, where we revealed PIK3Cδ as a prognostic factor for outcomes (OS and DFS), providing strong evidence for the use of PIK3Cδ inhibitors in this setting in clinical trials. Interestingly, PIK3Cδ was also expressed in the cancer cell population of patients, possibly as a result of inflammatory processes, since it has been reported that PIK3Cδ can be activated by pro-inflammatory mediators (70). This can explain the low/undetectable protein levels of PIK3Cδ in our tested BC cell lines and in our animal models, considering the short period of the *in vivo* experiments. In light of new evidence of the existence of distinct TNBC subtypes (71, 72), an even more comprehensive profiling of TNBC patients can reveal a specific subgroup where stromal/tumoral PIK3Cδ can epitomize a successful treatment strategy.

In conclusion, this study highlights the so-far undescribed tumor promoting role of fibroblast-expressed PIK3Cδ in BC. Although our work predominantly focused on TNBC, fibroblasts represent the major cellular components within the TME in most cancers, therefore the involvement of PIK3Cδ in other BC subtypes and malignancies should be explored. Considering that local invasion and metastasis are the main causes of death for most types of cancer, this discovery opens new potential therapeutic paths and supports the rationale for using PIK3Cδ inhibitors (as single or combined therapy) for the treatment of solid tumors where irregular activation of stromal PIK3Cδ occurs independently of the immunological landscape.

Funding

This work was supported by the Imperial BRC and ECMC, Action Against Cancer, The Colin MacDavid Family Trust, The Joseph Ettedgui Charitable Foundation, Mr Alessandro Dusi and Mr Julian and Mrs Cat O'Dell. BSRC "Alexander Fleming" work was supported by InfrafrontierGR/Phenotypos (MIS 5002135) implemented under the Actions Reinforcement of the Research and Innovation funded by the Operational Programme Competitiveness, Entrepreneurship and Innovation (NSRF 2014-2020) and co-financed by Greece and the European Union (European Regional Development Fund).

Acknowledgments

We would like to thank Margarita Andreadou for her help with the histology analysis and the Nottingham Health Science Biobank for the provision of tissue samples. A special thank you to Athanasios Giamas for helping with the preparation of the figures. The authors acknowledge the role of the Breast Cancer Now Tissue Bank in collecting and making available the samples used in the generation of this publication. We thank Michael Toss for his assistance with histopathology and Rosy Favicchio for the useful and stimulating discussions. We would like to thank Enrico Frabetti for his endless patience and support.

Competing interest

Professor Stebbing sits on SABs for Celltrion, Singapore Biotech, Vor Biopharma, TLC Biopharmaceuticals and Benevolent AI, has consulted with Lansdowne partners, Vitruvian and Social Impact Capital and Chairs the Board of Directors for BB Biotech Healthcare Trust and Xerion Healthcare.

Authors' contributionT.G. and G.G. conceived the project and participated in the study design, planned and oversaw the execution of all the work, collated and analyzed most of the data, interpreted the results and wrote most of the manuscript. A.D, V.V., K.B., G.B., performed most of the biochemical and cell-based experiments described herein. K.S., T.O'H., K.K., L.Li. and M.D. performed the RNAseq experiments and contributed in the interpretation of the results and writing the respective parts of the manuscript. K.S, performed the secretome data analysis and the TCGA deconvolution analysis. S.G., V.N. and D.L.K. performed the xenograft mouse model and the respective IHC analyses. L.La, J.C., P.H., E.S. performed all

the experiments related to the MMTV-PyMT transgenic mouse model. P.C., G.BH and F.M.G.P. performed the bioinformatic analysis related to the siRNA screening experiment. M.A., E.A.R. and A.R.G., performed the IHC staining and analyses on the TNBC patients' cohort and analyzed the data. K.Y. and S.C.L performed the IHC on ER^+ patients' cohort and analyzed the data. J.S. assisted with the interpretation of the clinical data and edited the manuscript. All authors read and approved the final manuscript.

Materials and methods

Ethics approval

This work obtained ethics approval by the North West – Greater Manchester Central Research Ethics Committee under the title; Nottingham Health Science Biobank (NHSB), reference number 15/NW/0685.

For all other information please refer to Supplementary information.

References

1. Bauer KR, Brown M, Cress RD, Parise CA, Caggiano V. Descriptive analysis of estrogen receptor (ER)-negative, progesterone receptor (PR)-negative, and HER2-negative invasive breast cancer, the so-called triple-negative phenotype: a population-based study from the California cancer Registry. Cancer. 2007;109(9):1721-8.
2. Perou CM, Sorlie T, Eisen MB, van de Rijn M, Jeffrey SS, Rees CA, et al. Molecular portraits of human breast tumours. Nature. 2000;406(6797):747-52.
3. Joyce JA, Pollard JW. Microenvironmental regulation of metastasis. Nat Rev Cancer. 2009;9(4):239-52.
4. Kalluri R, Zeisberg M. Fibroblasts in cancer. Nat Rev Cancer. 2006;6(5):392-401.
5. Quail DF, Joyce JA. Microenvironmental regulation of tumor progression and metastasis. Nat Med. 2013;19(11):1423-37.
6. Bhowmick NA, Moses HL. Tumor-stroma interactions. Curr Opin Genet Dev. 2005;15(1):97-101.
7. Finak G, Bertos N, Pepin F, Sadekova S, Souleimanova M, Zhao H, et al. Stromal gene expression predicts clinical outcome in breast cancer. Nat Med. 2008;14(5):518-27.
8. Costa A, Kieffer Y, Scholer-Dahirel A, Pelon F, Bourachot B, Cardon M, et al. Fibroblast Heterogeneity and Immunosuppressive Environment in Human Breast Cancer. Cancer cell. 2018;33(3):463-79 e10.
9. West RB, Nuyten DS, Subramanian S, Nielsen TO, Corless CL, Rubin BP, et al. Determination of stromal signatures in breast carcinoma. PLoS Biol. 2005;3(6):e187.
10. McAllister SS, Weinberg RA. Tumor-host interactions: a far-reaching relationship. J Clin Oncol. 2010;28(26):4022-8.
11. Parsonage G, Filer AD, Haworth O, Nash GB, Rainger GE, Salmon M, et al. A stromal address code defined by fibroblasts. Trends Immunol. 2005;26(3):150-6.
12. Tomasek JJ, Gabbiani G, Hinz B, Chaponnier C, Brown RA. Myofibroblasts and mechano-regulation of connective tissue remodelling. Nat Rev Mol Cell Biol. 2002;3(5):349-63.
13. Lu P, Weaver VM, Werb Z. The extracellular matrix: a dynamic niche in cancer progression. J Cell Biol. 2012;196(4):395-406.
14. McMillin DW, Negri JM, Mitsiades CS. The role of tumour-stromal interactions in modifying drug response: challenges and opportunities. Nat Rev Drug Discov. 2013;12(3):217-28.
15. Vanhaesebroeck B, Whitehead MA, Pineiro R. Molecules in medicine mini-review: isoforms of PI3K in biology and disease. J Mol Med (Berl). 2016;94(1):5-11.
16. De Henau O, Rausch M, Winkler D, Campesato LF, Liu C, Cymerman DH, et al. Overcoming resistance to checkpoint blockade therapy by targeting PI3Kgamma in myeloid cells. Nature. 2016;539(7629):443-7.
17. Koyasu S. The role of PI3K in immune cells. Nat Immunol. 2003;4(4):313-9.
18. Okkenhaug K, Graupera M, Vanhaesebroeck B. Targeting PI3K in Cancer: Impact on Tumor Cells, Their Protective Stroma, Angiogenesis, and Immunotherapy. Cancer Discov. 2016;6(10):1090-105.
19. Lucas CL, Kuehn HS, Zhao F, Niemela JE, Deenick EK, Palendira U, et al. Dominant-activating germline mutations in the gene encoding the PI(3)K catalytic subunit p110delta result in T cell senescence and human immunodeficiency. Nat Immunol. 2014;15(1):88-97.
20. Kang S, Denley A, Vanhaesebroeck B, Vogt PK. Oncogenic transformation induced by the p110beta, -gamma, and -delta isoforms of class I phosphoinositide 3-kinase. Proc Natl Acad Sci U S A. 2006;103(5):1289-94.
21. Tzenaki N, Papakonstanti EA. p110delta PI3 kinase pathway: emerging roles in cancer. Front Oncol. 2013;3:40.

22. Conte E, Fruciano M, Fagone E, Gili E, Caraci F, Iemmolo M, et al. Inhibition of PI3K prevents the proliferation and differentiation of human lung fibroblasts into myofibroblasts: the role of class I P110 isoforms. PloS one. 2011;6(10):e24663.
23. Puri KD, Doggett TA, Douangpanya J, Hou Y, Tino WT, Wilson T, et al. Mechanisms and implications of phosphoinositide 3-kinase delta in promoting neutrophil trafficking into inflamed tissue. Blood. 2004;103(9):3448-56.
24. Erdmann T, Klener P, Lynch JT, Grau M, Vockova P, Molinsky J, et al. Sensitivity to PI3K and AKT inhibitors is mediated by divergent molecular mechanisms in subtypes of DLBCL. Blood. 2017;130(3):310-22.
25. Karbownik MS, Szemraj J, Wieteska L, Antczak A, Gorski P, Kowalczyk E, et al. Antipsychotic Drugs Differentially Affect mRNA Expression of Genes Encoding the Neuregulin 1-Downstream ErbB4-PI3K Pathway. Pharmacology. 2016;98(1-2):4-12.
26. Vogel C, Marcotte EM. Insights into the regulation of protein abundance from proteomic and transcriptomic analyses. Nat Rev Genet. 2012;13(4):227-32.
27. Uhlen M, Fagerberg L, Hallstrom BM, Lindskog C, Oksvold P, Mardinoglu A, et al. Proteomics. Tissue-based map of the human proteome. Science. 2015;347(6220):1260419.
28. Lee JY, Hong SH, Shin M, Heo HR, Jang IH. Blockade of FLT4 suppresses metastasis of melanoma cells by impaired lymphatic vessels. Biochem Biophys Res Commun. 2016;478(2):733-8.
29. Owusu BY, Thomas S, Venukadasula P, Han Z, Janetka JW, Galemmo RA, Jr., et al. Targeting the tumor-promoting microenvironment in MET-amplified NSCLC cells with a novel inhibitor of pro-HGF activation. Oncotarget. 2017;8(38):63014-25.
30. Togashi Y, Sakamoto H, Hayashi H, Terashima M, de Velasco MA, Fujita Y, et al. Homozygous deletion of the activin A receptor, type IB gene is associated with an aggressive cancer phenotype in pancreatic cancer. Mol Cancer. 2014;13:126.
31. Orzan F, De Bacco F, Crisafulli G, Pellegatta S, Mussolin B, Siravegna G, et al. Genetic Evolution of Glioblastoma Stem-Like Cells From Primary to Recurrent Tumor. Stem Cells. 2017;35(11):2218-28.
32. Hoellenriegel J, Meadows SA, Sivina M, Wierda WG, Kantarjian H, Keating MJ, et al. The phosphoinositide 3'-kinase delta inhibitor, CAL-101, inhibits B-cell receptor signaling and chemokine networks in chronic lymphocytic leukemia. Blood. 2011;118(13):3603-12.
33. Jacob J, Favicchio R, Karimian N, Mehrabi M, Harding V, Castellano L, et al. LMTK3 escapes tumour suppressor miRNAs via sequestration of DDX5. Cancer Lett. 2016;372(1):137-46.
34. Bochet L, Lehuede C, Dauvillier S, Wang YY, Dirat B, Laurent V, et al. Adipocyte-derived fibroblasts promote tumor progression and contribute to the desmoplastic reaction in breast cancer. Cancer Res. 2013;73(18):5657-68.
35. Soon PS, Kim E, Pon CK, Gill AJ, Moore K, Spillane AJ, et al. Breast cancer-associated fibroblasts induce epithelial-to-mesenchymal transition in breast cancer cells. Endocr Relat Cancer. 2013;20(1):1-12.
36. Stebbing J, Shah K, Lit LC, Gagliano T, Ditsiou A, Wang T, et al. LMTK3 confers chemo-resistance in breast cancer. Oncogene. 2018.
37. Wu H, Bi J, Peng Y, Huo L, Yu X, Yang Z, et al. Nuclear receptor NR4A1 is a tumor suppressor down-regulated in triple-negative breast cancer. Oncotarget. 2017;8(33):54364-77.
38. Zhan Y, Du X, Chen H, Liu J, Zhao B, Huang D, et al. Cytosporone B is an agonist for nuclear orphan receptor Nur77. Nat Chem Biol. 2008;4(9):548-56.
39. Zhao S, Zhou L, Niu G, Li Y, Zhao D, Zeng H. Differential regulation of orphan nuclear receptor TR3 transcript variants by novel vascular growth factor signaling pathways. FASEB J. 2014;28(10):4524-33.

40. Zhou L, Cui P, Zhao S, Ye T, Li Y, Peng J, et al. Differential function and regulation of orphan nuclear receptor TR3 isoforms in endothelial cells. Tumour Biol. 2016;37(3):3307-20.
41. Kuribara M, Kidane AH, Vos GA, de Gouw D, Roubos EW, Scheenen WJ, et al. Extracellular-signal regulated kinase regulates production of pro-opiomelanocortin in pituitary melanotroph cells. Journal of neuroendocrinology. 2011;23(3):261-8.
42. Liu D, Jia H, Holmes DI, Stannard A, Zachary I. Vascular endothelial growth factor-regulated gene expression in endothelial cells: KDR-mediated induction of Egr3 and the related nuclear receptors Nur77, Nurr1, and Nor1. Arteriosclerosis, thrombosis, and vascular biology. 2003;23(11):2002-7.
43. Su YT, Gao C, Liu Y, Guo S, Wang A, Wang B, et al. Monoubiquitination of filamin B regulates vascular endothelial growth factor-mediated trafficking of histone deacetylase 7. Molecular and cellular biology. 2013;33(8):1546-60.
44. Xu L, Cochran DM, Tong RT, Winkler F, Kashiwagi S, Jain RK, et al. Placenta growth factor overexpression inhibits tumor growth, angiogenesis, and metastasis by depleting vascular endothelial growth factor homodimers in orthotopic mouse models. Cancer research. 2006;66(8):3971-7.
45. Hondermarck H. Neurotrophins and their receptors in breast cancer. Cytokine & growth factor reviews. 2012;23(6):357-65.
46. Rajaram M, Li J, Egeblad M, Powers RS. System-wide analysis reveals a complex network of tumor-fibroblast interactions involved in tumorigenicity. PLoS Genet. 2013;9(9):e1003789.
47. Guy CT, Cardiff RD, Muller WJ. Induction of mammary tumors by expression of polyomavirus middle T oncogene: a transgenic mouse model for metastatic disease. Mol Cell Biol. 1992;12(3):954-61.
48. Abd El-Rehim DM, Ball G, Pinder SE, Rakha E, Paish C, Robertson JF, et al. High-throughput protein expression analysis using tissue microarray technology of a large well-characterised series identifies biologically distinct classes of breast cancer confirming recent cDNA expression analyses. Int J Cancer. 2005;116(3):340-50.
49. Blamey RW, Ellis IO, Pinder SE, Lee AH, Macmillan RD, Morgan DA, et al. Survival of invasive breast cancer according to the Nottingham Prognostic Index in cases diagnosed in 1990-1999. Eur J Cancer. 2007;43(10):1548-55.
50. Adams S, Schmid P, Rugo HS, Winer EP, Loirat D, Awada A, et al. Pembrolizumab Monotherapy for Previously Treated Metastatic Triple-Negative Breast Cancer: Cohort A of the Phase 2 KEYNOTE-086 Study. Annals of oncology : official journal of the European Society for Medical Oncology. 2018.
51. Bardia A, Mayer IA, Vahdat LT, Tolaney SM, Isakoff SJ, Diamond JR, et al. Sacituzumab Govitecan-hziy in Refractory Metastatic Triple-Negative Breast Cancer. The New England journal of medicine. 2019;380(8):741-51.
52. Bianchini G, Balko JM, Mayer IA, Sanders ME, Gianni L. Triple-negative breast cancer: challenges and opportunities of a heterogeneous disease. Nature reviews Clinical oncology. 2016;13(11):674-90.
53. Nanda R, Chow LQ, Dees EC, Berger R, Gupta S, Geva R, et al. Pembrolizumab in Patients With Advanced Triple-Negative Breast Cancer: Phase Ib KEYNOTE-012 Study. Journal of clinical oncology : official journal of the American Society of Clinical Oncology. 2016;34(21):2460-7.
54. Henderson IC, Berry DA, Demetri GD, Cirrincione CT, Goldstein LJ, Martino S, et al. Improved outcomes from adding sequential Paclitaxel but not from escalating Doxorubicin dose in an adjuvant chemotherapy regimen for patients with node-positive primary breast

cancer. Journal of clinical oncology : official journal of the American Society of Clinical Oncology. 2003;21(6):976-83.
55. Sounni NE, Noel A. Targeting the tumor microenvironment for cancer therapy. Clin Chem. 2013;59(1):85-93.
56. Blume-Jensen P, Hunter T. Oncogenic kinase signalling. Nature. 2001;411(6835):355-65.
57. Giamas G, Man YL, Hirner H, Bischof J, Kramer K, Khan K, et al. Kinases as targets in the treatment of solid tumors. Cell Signal. 2010;22(7):984-1002.
58. Krause DS, Van Etten RA. Tyrosine kinases as targets for cancer therapy. N Engl J Med. 2005;353(2):172-87.
59. Lemmon MA, Schlessinger J. Cell signaling by receptor tyrosine kinases. Cell. 2010;141(7):1117-34.
60. Stebbing J, Zhang H, Xu Y, Grothey A, Ajuh P, Angelopoulos N, et al. Characterization of the Tyrosine Kinase-Regulated Proteome in Breast Cancer by Combined use of RNA interference (RNAi) and Stable Isotope Labeling with Amino Acids in Cell Culture (SILAC) Quantitative Proteomics. Mol Cell Proteomics. 2015;14(9):2479-92.
61. Somoza JR, Koditek D, Villasenor AG, Novikov N, Wong MH, Liclican A, et al. Structural, biochemical, and biophysical characterization of idelalisib binding to phosphoinositide 3-kinase delta. J Biol Chem. 2015;290(13):8439-46.
62. Boudreaux SP, Duren RP, Call SG, Nguyen L, Freire PR, Narayanan P, et al. Drug targeting of NR4A nuclear receptors for treatment of acute myeloid leukemia. Leukemia. 2019;33(1):52-63.
63. Close AF, Dadheech N, Villela BS, Rouillard C, Buteau J. The orphan nuclear receptor Nor1/Nr4a3 is a negative regulator of beta-cell mass. J Biol Chem. 2019;294(13):4889-97.
64. Medunjanin S, Daniel JM, Weinert S, Dutzmann J, Burgbacher F, Brecht S, et al. DNA-dependent protein kinase (DNA-PK) permits vascular smooth muscle cell proliferation through phosphorylation of the orphan nuclear receptor NOR1. Cardiovasc Res. 2015;106(3):488-97.
65. Munnur D, Somers J, Skalka G, Weston R, Jukes-Jones R, Bhogadia M, et al. NR4A Nuclear Receptors Target Poly-ADP-Ribosylated DNA-PKcs Protein to Promote DNA Repair. Cell Rep. 2019;26(8):2028-36 e6.
66. Safe S, Jin UH, Morpurgo B, Abudayyeh A, Singh M, Tjalkens RB. Nuclear receptor 4A (NR4A) family - orphans no more. J Steroid Biochem Mol Biol. 2016;157:48-60.
67. Kalluri R. The biology and function of fibroblasts in cancer. Nature reviews Cancer. 2016;16(9):582-98.
68. Chomarat P, Banchereau J, Davoust J, Palucka AK. IL-6 switches the differentiation of monocytes from dendritic cells to macrophages. Nat Immunol. 2000;1(6):510-4.
69. Erez N, Truitt M, Olson P, Arron ST, Hanahan D. Cancer-Associated Fibroblasts Are Activated in Incipient Neoplasia to Orchestrate Tumor-Promoting Inflammation in an NF-kappaB-Dependent Manner. Cancer Cell. 2010;17(2):135-47.
70. Whitehead MA, Bombardieri M, Pitzalis C, Vanhaesebroeck B. Isoform-selective induction of human p110delta PI3K expression by TNFalpha: identification of a new and inducible PIK3CD promoter. The Biochemical journal. 2012;443(3):857-67.
71. Jiang YZ, Ma D, Suo C, Shi J, Xue M, Hu X, et al. Genomic and Transcriptomic Landscape of Triple-Negative Breast Cancers: Subtypes and Treatment Strategies. Cancer cell. 2019.
72. Rueda OM, Sammut SJ, Seoane JA, Chin SF, Caswell-Jin JL, Callari M, et al. Dynamics of breast-cancer relapse reveal late-recurring ER-positive genomic subgroups. Nature. 2019.

Figure 1

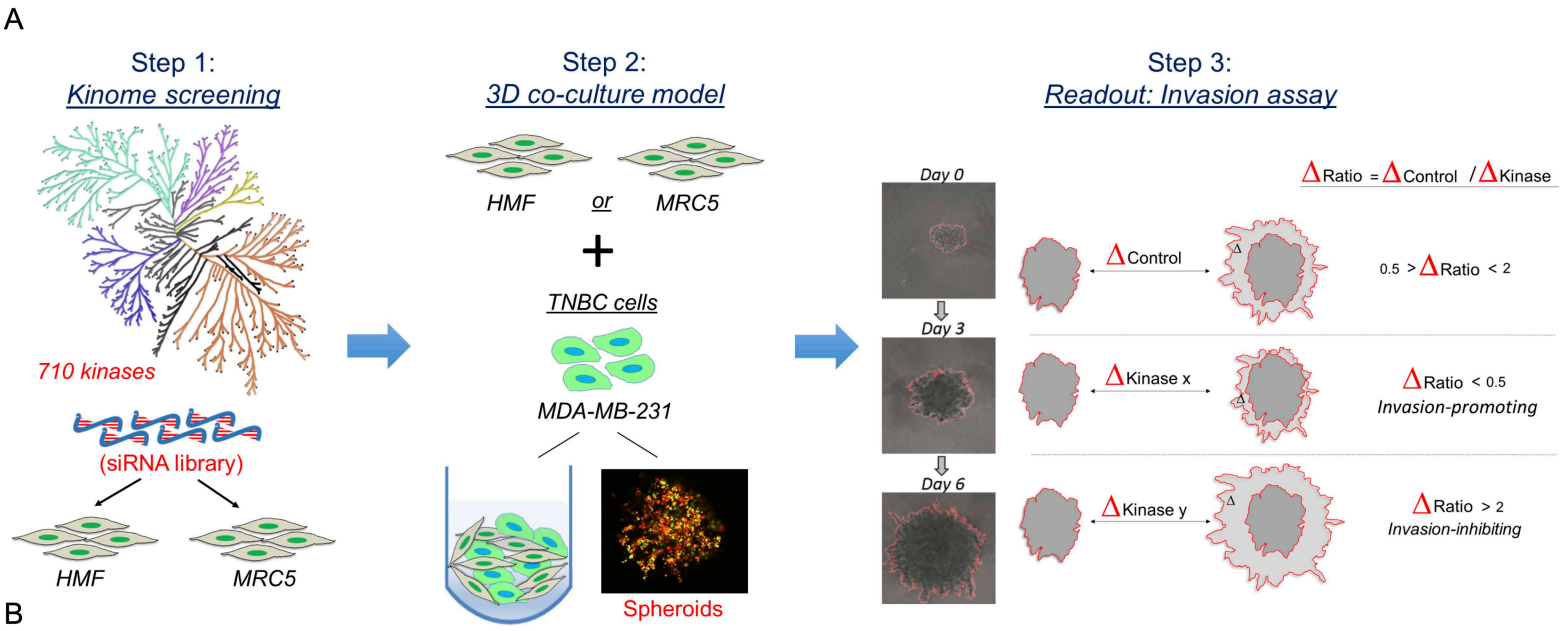
A
Step 1:
Kinome screening
710 kinases
(siRNA library)
HMF
MRC5
Step 2:
3D co-culture model
HMF
or
MRC5
+
TNBC cells
MDA-MB-231
Spheroids
Step 3:
Readout: Invasion assay
Day 0
Day 3
Day 6
ΔRatio = ΔControl / ΔKinase
ΔControl
0.5 > ΔRatio < 2
ΔKinase x
ΔRatio < 0.5
Invasion-promoting
ΔKinase y
ΔRatio > 2
Invasion-inhibiting

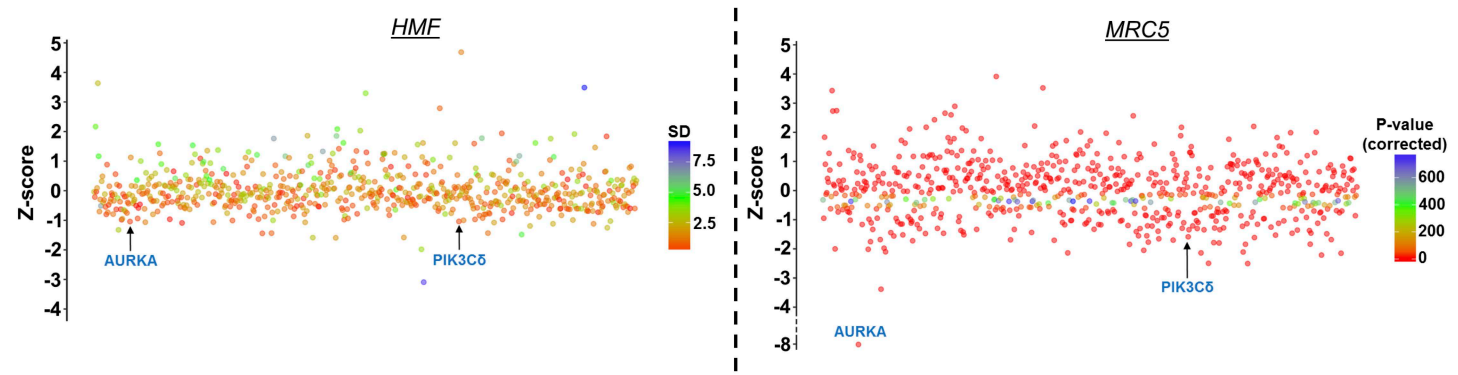
B
Step 4: Data analysis
HMF
MRC5
Z-score
SD
7.5
5.0
2.5
P-value
(corrected)
600
400
200
0
AURKA
PIK3Cδ

Figure 1: Experimental design of siRNA Kinome screening and identification of fibroblast-expressed kinases affecting TNBC invasion.

(A) *Step 1*: Silencing of 710 kinases in HMF and MRC5 cells using a siRNA kinome library. *Step 2*: 3D co-culture of HMF or MRC5 with MDA-MB-231 in the presence of Matrigel® and chemoattractants to promote invasion. A representative image of cells stained with different fluorescent lipophilic tracers is shown: MDA-MB-231 (red/ DiRDiIC18) and MRC5 (green/DiOC6). *Step 3*: The invasive potential of MDA-MB-231 cells was used as a readout tool. Results are expressed as changes in spheroid surface between Day 6 and Day 3 (Δ_{Ratio}= Δ_{CT}/Δ_{K}). The Δ_{Ratio} values were used to calculate the Z-Scores based on the formula: $\mathbf{z = (x - \mu)/\sigma}$ ($\boldsymbol{\mu}$: Δ_{Ratio} mean of 710 kinases; $\boldsymbol{\sigma}$: standard deviation (SD); **x**: Δ_{Ratio} value for each kinase). For HMF, the Δ_{Ratio} Z-Score colour code refers to SD, as the screening was performed twice, while for MRC-5 the Δ_{Ratio} Z-Score colour code refers to p-Value. (**B**) *Step 4*: The Z-Score for HMF and MRC5 are shown. Kinases were divided depending on their effects on MDA-MB-231 invasion. 'Invasion-promoting': $\Delta_{Ratio} \leq 0.5$, $P < 0.01$ (as well as SD < 0.5 for HMF). 'Invasion inhibiting': $\Delta_{Ratio} > 2$, $P > 0.05$ (as well as SD>0.5 for HMF).

Figure 2

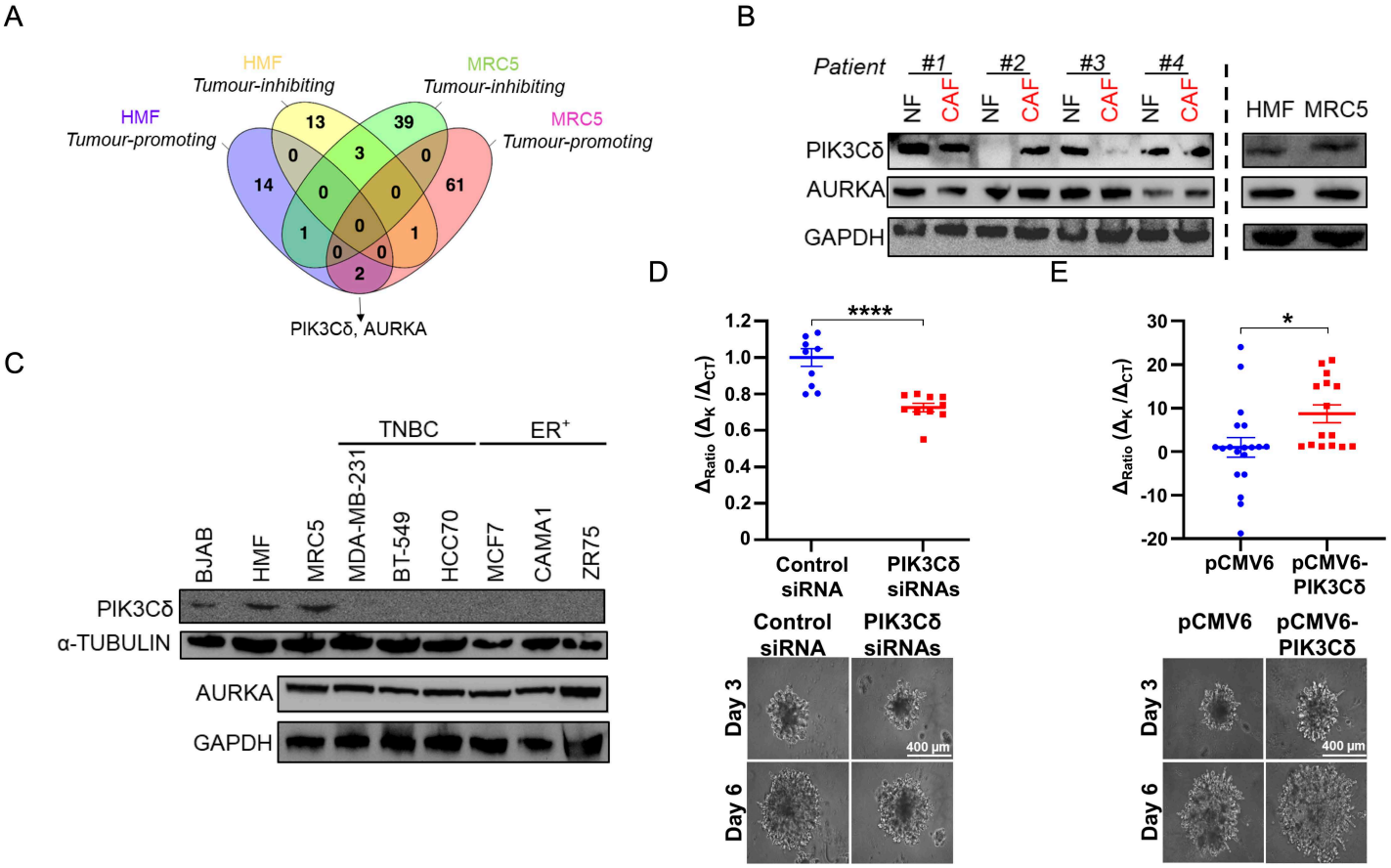
A
HMF
Tumour-inhibiting
MRC5
Tumour-inhibiting
HMF
Tumour-promoting
MRC5
Tumour-promoting
13
39
0
3
0
14
0
0
61
0
1
0
1
0
0
2
PIK3Cδ, AURKA
B
Patient
#1
#2
#3
#4
NF
CAF
NF
CAF
NF
CAF
NF
CAF
HMF
MRC5
PIK3Cδ
AURKA
GAPDH
C
TNBC
ER+
BJAB
HMF
MRC5
MDA-MB-231
BT-549
HCC70
MCF7
CAMA1
ZR75
PIK3Cδ
α-TUBULIN
AURKA
GAPDH
D
E
****
*
Control siRNA
PIK3Cδ siRNAs
pCMV6
pCMV6-PIK3Cδ
Day 3
Day 6
400 µm

Figure 2: Involvement of fibroblast-expressed PIK3Cδ in TNBC invasion.

(A) Venn diagrams comparing the number of invasion-promoting and invasion-inhibiting kinases in HMF and MRC5 cells. (**B**) Western blotting of PIK3Cδ and AURKA in HMF, MRC5 and primary fibroblasts obtained from TNBC patients. GADPH was used as loading control. (**C**) Western blotting of PIK3Cδ and AURKA in BC and fibroblast cell lines (BJAB B-cell-line were used as positive control for PIK3Cδ expression). GADPH and α-tubulin were used as loading controls. (**D**) Validation of effects of PIK3Cδ knockdown in MRC5 on MDA-MB-231 invasion following the experimental procedure described above (*n*=3 independent experiments, minimum 3 technical replicates). Results are expressed as mean ± SEM. Significance was calculated using unpaired t-test; **** $P < 0.0001$ vs Control siRNA. (**E**). Effects of PIK3Cδ overexpression in MRC5, using pCMV6-AC-PIK3Cδ-GFP plasmid, on MDA-MB-231 invasion following the experimental procedure described above (*n*=3 independent experiments, minimum 3 technical replicates). Results are expressed as mean ± SEM. Significance was calculated using unpaired t-test; * $P < 0.05$ vs Control siRNA vs pCMV6 transfected fibroblasts.

Figure 3

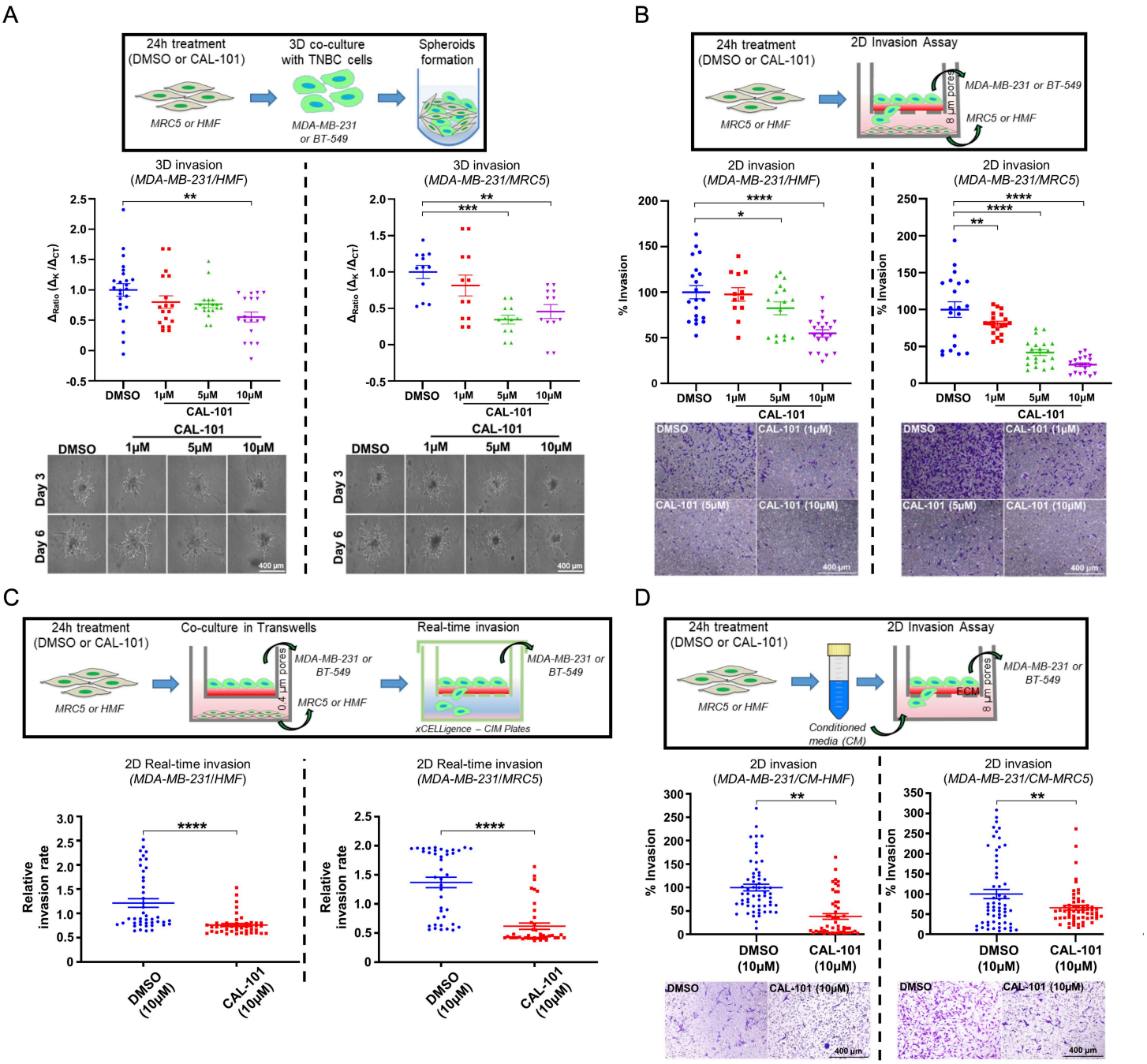
A
24h treatment (DMSO or CAL-101)
3D co-culture with TNBC cells
Spheroids formation
MRC5 or HMF
MDA-MB-231 or BT-549
3D invasion (MDA-MB-231/HMF)
3D invasion (MDA-MB-231/MRC5)
CAL-101
DMSO
1μM
5μM
10μM
Day 3
Day 6
400 μm
B
24h treatment (DMSO or CAL-101)
2D Invasion Assay
8 μm pores
2D invasion (MDA-MB-231/HMF)
2D invasion (MDA-MB-231/MRC5)
% Invasion
CAL-101 (1μM)
CAL-101 (5μM)
CAL-101 (10μM)
C
24h treatment (DMSO or CAL-101)
Co-culture in Transwells
0.4 μm pores
Real-time invasion
xCELLigence – CIM Plates
2D Real-time invasion (MDA-MB-231/HMF)
2D Real-time invasion (MDA-MB-231/MRC5)
Relative invasion rate
D
24h treatment (DMSO or CAL-101)
2D Invasion Assay
Conditioned media (CM)
ECM
2D invasion (MDA-MB-231/CM-HMF)
2D invasion (MDA-MB-231/CM-MRC5)

Figure 3: Effects of chemical inhibition of PIK3Cδ on TNBC 2D and 3D invasion.

(A) 3D invasion assay: HMF (left panel) and MRC5 (right panel) were pre-treated with DMSO or with 1/5/10 µM of CAL-101. After 24h, fibroblasts were co-cultured with MDA-MB-231 and invasion was measured. Representative pictures are shown (*n*=3 independent experiments, minimum 4 technical replicates). Significance was calculated using one-way Anova and Tukey's multiple comparisons tests. Results are expressed as mean ± SEM; ** P < 0.01, *** P < 0.001 vs DMSO treated fibroblasts. (**B**) 2D invasion assay: HMF (left panel) and MRC5 (right panel) were pre-treated with DMSO or with 1/5/10 µM of CAL-101 for 24h and were seeded on the lower chamber of a transwell. MDA-MB-231 cells were seeded on the Matrigel-coated upper chamber of the transwell and co-cultured with the fibroblasts. 24h later, migrated MDA-MB-231 cells were fixed, stained and counted (n=3 independent experiments, minimum 3 technical replicates) Significance was calculated using one-way Anova and Tukey's multiple comparisons tests. Data are expressed as mean ± SEM; * P < 0.05, ** P < 0.01, **** P < 0.0001 vs DMSO treated fibroblasts. (**C**) Real-time invasion assay: HMF (left panel) and MRC5 (right panel) were treated as mentioned in 2B. MDA-MB-231 cells were seeded on the upper chamber of the transwell insert and were co-cultured with the fibroblasts. After 24h, MDA-MB-231 were moved to CIM-Plates to monitor their relative invasion rate t. Significance was calculated using unpaired t-test. Results are expressed as mean ± SEM; **** P < 0.0001. **(D)** Conditioned Medium (CM) invasion assay: HMF (left panel) and MRC5 (right panel) were treated with vehicle or with 10 µM CAL-101 in serum free for 24h to obtain the CM. MDA-MB-231 were incubated with HMF or MRC5 CM for 2D invasion assays (n=3 independent experiments, minimum 10 technical replicates). Significance was calculated using unpaired t-test. Data are expressed as mean ± SEM; ** P < 0.01 vs DMSO-treated fibroblasts' CM.

Figure 4

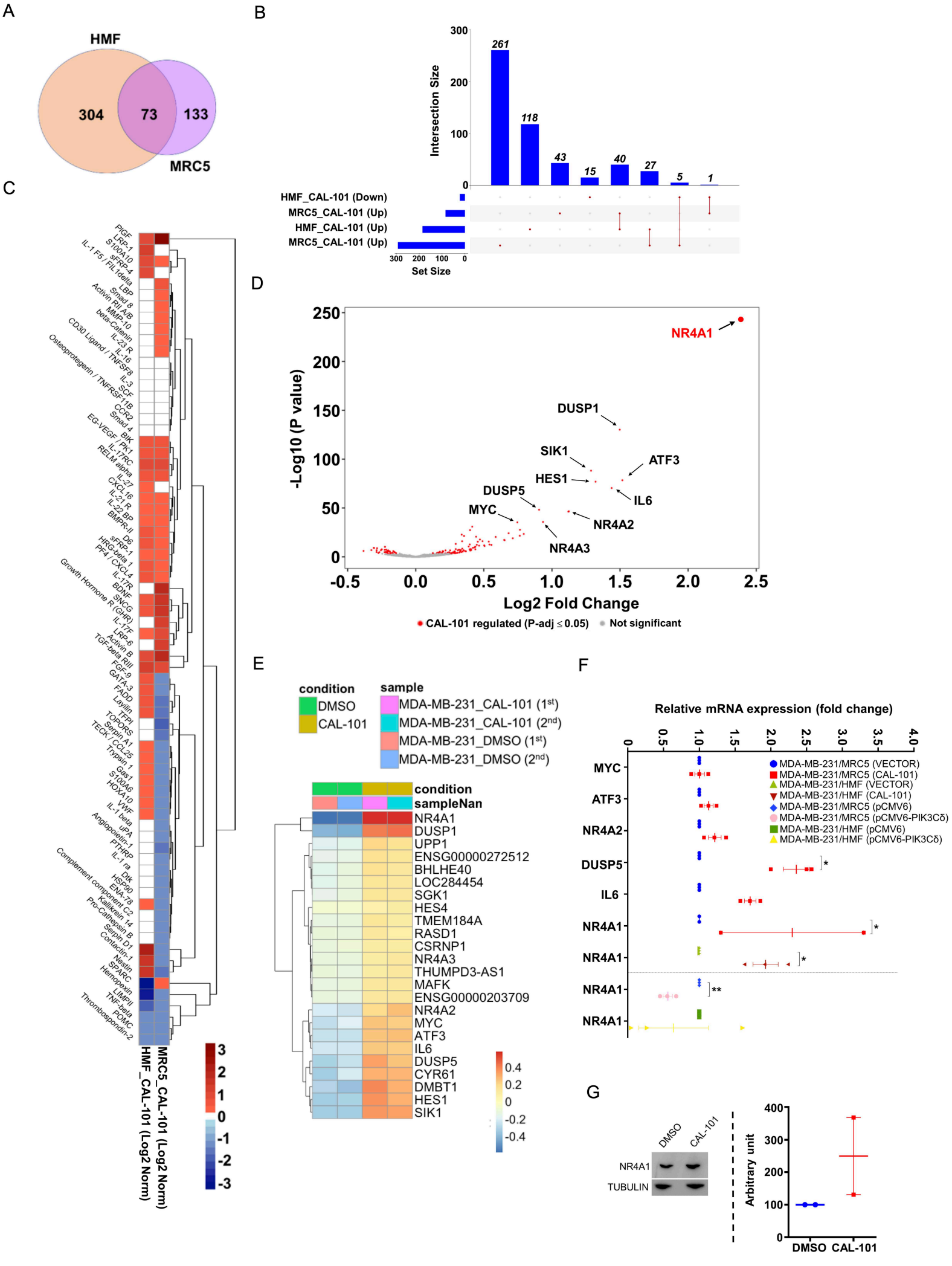
A
HMF
304
73
133
MRC5
B
Intersection Size
261
118
43
15
40
27
5
1
HMF_CAL-101 (Down)
MRC5_CAL-101 (Up)
HMF_CAL-101 (Up)
MRC5_CAL-101 (Up)
Set Size
C
HMF_CAL-101 (Log2 Norm)
MRC5_CAL-101 (Log2 Norm)
D
-Log10 (P value)
Log2 Fold Change
NR4A1
DUSP1
SIK1
ATF3
HES1
IL6
DUSP5
MYC
NR4A2
NR4A3
CAL-101 regulated (P-adj ≤ 0.05)
Not significant
E
condition
DMSO
CAL-101
sample
MDA-MB-231_CAL-101 (1st)
MDA-MB-231_CAL-101 (2nd)
MDA-MB-231_DMSO (1st)
MDA-MB-231_DMSO (2nd)
F
Relative mRNA expression (fold change)
MDA-MB-231/MRC5 (VECTOR)
MDA-MB-231/MRC5 (CAL-101)
MDA-MB-231/HMF (VECTOR)
MDA-MB-231/HMF (CAL-101)
MDA-MB-231/MRC5 (pCMV6)
MDA-MB-231/MRC5 (pCMV6-PIK3Cδ)
MDA-MB-231/HMF (pCMV6)
MDA-MB-231/HMF (pCMV6-PIK3Cδ)
G
DMSO
CAL-101
NR4A1
TUBULIN
Arbitrary unit

Figure 4: Global secretome analysis of CAL-101 treated fibroblasts and transcriptomics analysis of MDA-MB-231 cells.

(**A**) To obtain CM from HMF and MRC5, cells were treated with vehicle or 10 μM CAL-101 in serum free medium for 24h. CM was used to perform secretome analysis using the Human L1000 array. Venn diagram showing differences in the secreted proteins significantly regulated by CAL-101 in HMF and MRC5 cells (Padj < 0.05 and Log2 fold difference of ≥|0.5|) (**B**) UpSet plot showing common and unique CAL-101 regulated proteins significantly up (Up) or down-regulated (Down) in each dataset (MRC5 and HMF). (**C**) Heatmap comparing Log2 fold change of secreted proteins between CAL-101 treated HMF and MRC5 cells. (**D**) MRC5 were treated with either DMSO or with 10 μM CAL-101 for 24h hours. Following, cells were washed with PBS to remove the treatment and complete fresh medium was added to each well. 5 μm inserts containing MDA-MB-231 were then added in the well containing previously treated MRC5. 24h after co-culture, cancer cells were collected for RNA extraction and subsequent RNA sequencing. Volcano plot showing the Log2 fold change of genes in MDA-MB-231 cells that responded differently to CAL-101 treatment on MRC5 (DMSO:CAL-101). The Log10 of P value, for significance in fold change, is plotted on the y-axis. (**E**) Heatmap showing amounts by which the read counts of the top-24 (ordered based on Log2 fold change ≥ |0.5| and Padj value ≤ 0.05) regulated genes deviates from the genes' average across all the samples. (**F**) qRT-PCR validation of genes identified via the RNAseq and DESeq2 analysis. Significance was calculated using unpaired t-tests. Results are expressed as mean ± SEM; *P < 0.05 vs vector. (**G**) Western blotting of NR4A1 in MDA-MB-231 cells following co-culture with CAL-101 treated MRC5 cells. α-tubulin was used as loading control. Densitometry analysis of the blot is displayed as a ratio between CAL-101-treated vs DMSO-treated cells.

Figure 5

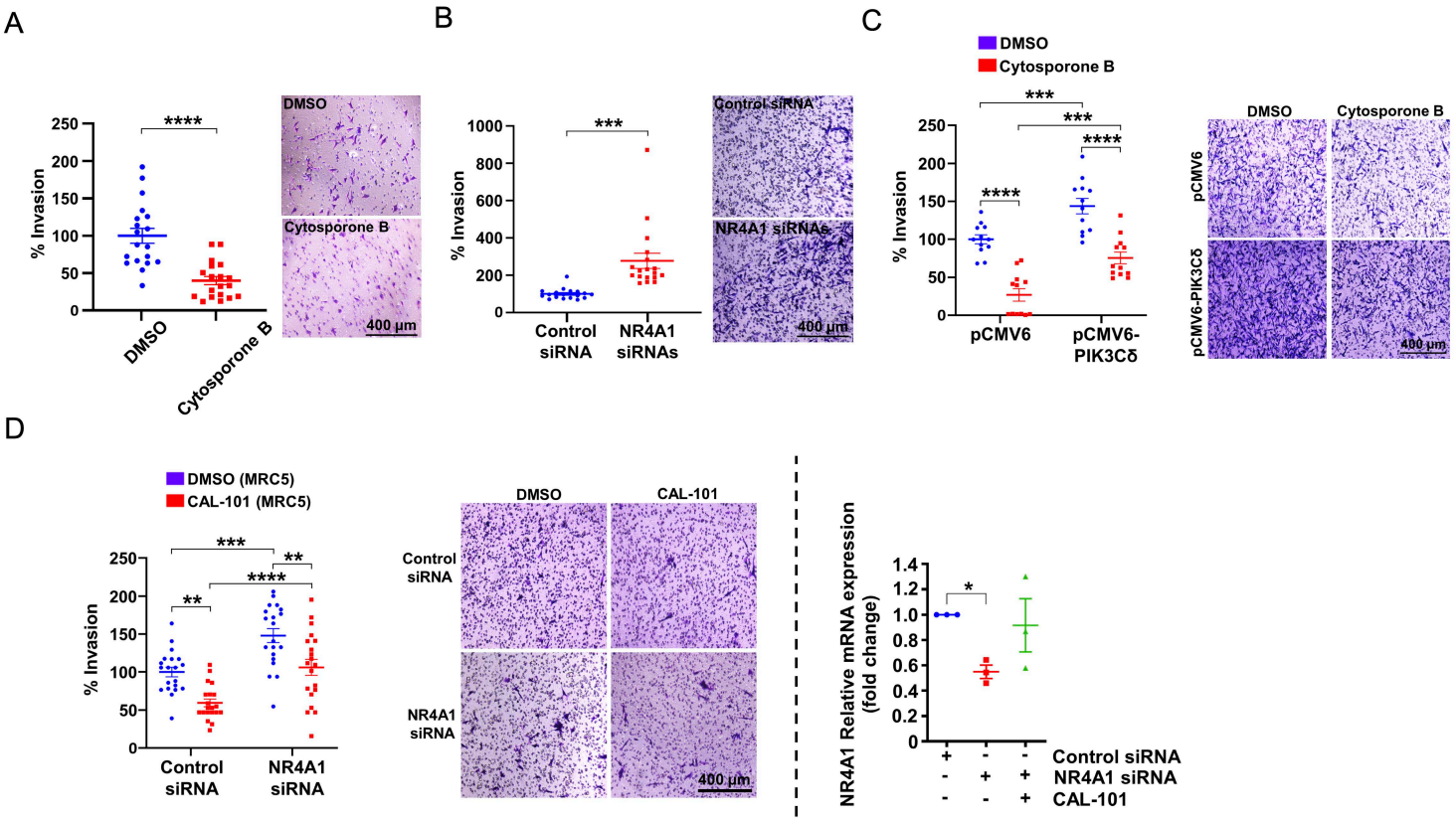
A
% Invasion
****
DMSO
Cytosporone B
400 µm
B
% Invasion
***
Control siRNA
NR4A1 siRNAs
400 µm
C
DMSO
Cytosporone B
% Invasion
***
***
****
****
pCMV6
pCMV6-PIK3Cδ
400 µm

D
DMSO (MRC5)
CAL-101 (MRC5)
% Invasion
***
**
****
**
Control siRNA
NR4A1 siRNA
DMSO
CAL-101
Control siRNA
NR4A1 siRNA
400 µm
NR4A1 Relative mRNA expression (fold change)
*
Control siRNA
NR4A1 siRNA
CAL-101

Figure 5: Effects of fibroblast PIK3Cδexpression on NR4A1-mediated invasion of TNBC cells.

(**A**) 2D invasion assay: MDA-MB-231 cells were seeded on the Matrigel-coated upper chamber of the transwell insert and were treated with DMSO or 5 μM Cytosporone B (CytoB). After 24h, migrated MDA-MB-231 cells were fixed, stained and counted (n=2 independent experiments, minimum 9 technical replicates). Significance was calculated using unpaired t-test. Results are expressed as mean ± SEM; **** $P < 0.0001$ vs. DMSO treated cells. (**B**) 2D invasion assay: MDA-MB-231 cells transfected with control or NR4A1 siRNAs were seeded as above. After 24h, migrated MDA-MB-231 cells were fixed, stained and counted (n=2 independent experiments, minimum 9 technical replicates). Significance was calculated using unpaired t-test. Results are expressed as mean ± SEM; *** $P < 0.001$ vs. siRNA control transfected cells. (**C**) Effects of PIK3Cδ overexpression in MRC5 on MDA-MB-231 invasion following pre-treatment of MDA-MB-231 with 5 μM CytoB. (n=2 independent experiments, minimum 9 technical replicates). Significance was calculated using two-way Anova and Tukey's multiple comparisons tests. Results are expressed as mean ± SEM; *** $P < 0.001$, **** $P < 0.0001$ vs the samples indicated in the graph. (**D**) Left/middle panels: MRC5 cells were treated with CAL-101 or DMSO. NR4A1-siRNA MDA-MB-231 or control-siRNA cells were seeded on the Matrigel-coated upper chamber of a transwell and co-cultured with fibroblasts. After 24h, migrated MDA-MB-231 cells were fixed, stained and counted (n=3 independent experiments, minimum 6 technical replicates). Significance was calculated using two-way Anova and Tukey's multiple comparisons tests. Results are expressed as mean ± SEM; ** $P < 0.01$, *** $P < 0.001$, **** $P < 0.0001$ vs the samples indicated in the graph. Right panel: NR4A1 levels were evaluated in siRNA transfected MDA-MB-231 before and after co-culture with CAL-101-treated MRC5. Significance was calculated using one-way ANOVA, followed by Dunnett's tests. Results are expressed as mean ± SEM; *$P < 0.05$ vs control.

Figure 6

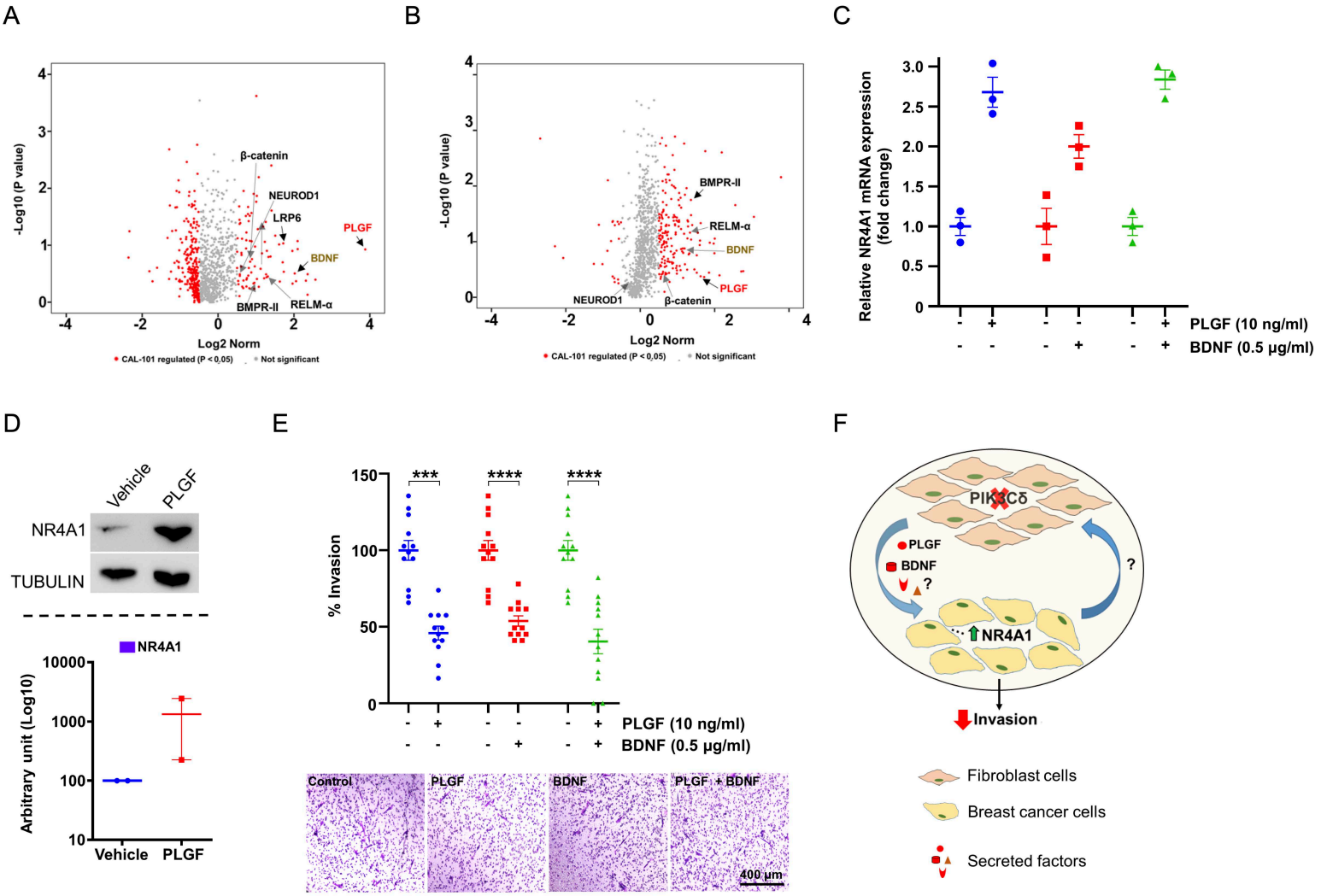
A
-Log10 (P value)
Log2 Norm
β-catenin
NEUROD1
LRP6
PLGF
BDNF
BMPR-II
RELM-α
CAL-101 regulated (P < 0,05)
Not significant
B
-Log10 (P value)
Log2 Norm
BMPR-II
RELM-α
BDNF
PLGF
NEUROD1
β-catenin
CAL-101 regulated (P < 0,05)
Not significant
C
Relative NR4A1 mRNA expression (fold change)
PLGF (10 ng/ml)
BDNF (0.5 µg/ml)
D
Vehicle
PLGF
NR4A1
TUBULIN
NR4A1
Arbitrary unit (Log10)
Vehicle
PLGF
E
% Invasion
***
****
****
PLGF (10 ng/ml)
BDNF (0.5 µg/ml)
Control
PLGF
BDNF
PLGF + BDNF
400 µm
F
PI3Kδ
PLGF
BDNF
?
?
NR4A1
Invasion
Fibroblast cells
Breast cancer cells
Secreted factors

Figure 6: Effects of PLGF/BDNF secreted factors on NR4A1-mediated invasion of TNBC cells.

(**A**) Volcano plot showing the Log2 fold change of secreted proteins in MRC5 cells that responded differentially to the CAL-101 treatment. The Log10 of P value, for significance in fold change, is plotted on the y-axis. **(B)** Volcano plot showing the Log2 fold change of secreted proteins in HMF cells that responded differentially to the CAL-101 treatment. The Log10 of P value, for significance in fold change, is plotted on the y-axis. (**C**) qRT-PCR of *NR4A1* expression levels in MDA-MB-231 cells following treatment with PLGF and BDNF. (**D**) Western blotting of NR4A1 in MDA-MB-231 cells following treatment with PLGF (10ng/ml). GAPDH was used as loading control. Densitometry analysis of the blot is displayed as a ratio between PLGF-treated vs vehicle-treated cells. (**E**) 2D invasion assay: MDA-MB-231 cells were seeded on the Matrigel-coated upper chamber of the transwell insert and were treated with PLGF or BDNF or vehicle. After 24h, migrated MDA-MB-231 cells were fixed, stained and counted (n=3 independent experiments, minimum 4 technical replicates). Significance was calculated using unpaired t-test. Results are expressed as mean ± SEM; *** $P < 0.001$, **** $P < 0.0001$ vs vehicle treated cells. (**F**) Schematic model depicting the paracrine signaling pathway between fibroblasts and TNBC cells. Inhibition of PIK3Cδ in fibroblasts leads to the secretion of different factors, including PLGF and BDNF, which promote the overexpression of *NR4A1* in epithelial cancer cells. NR4A1 acts as a tumor suppressor inhibiting the invasiveness of TNBC cells.

Figure 7

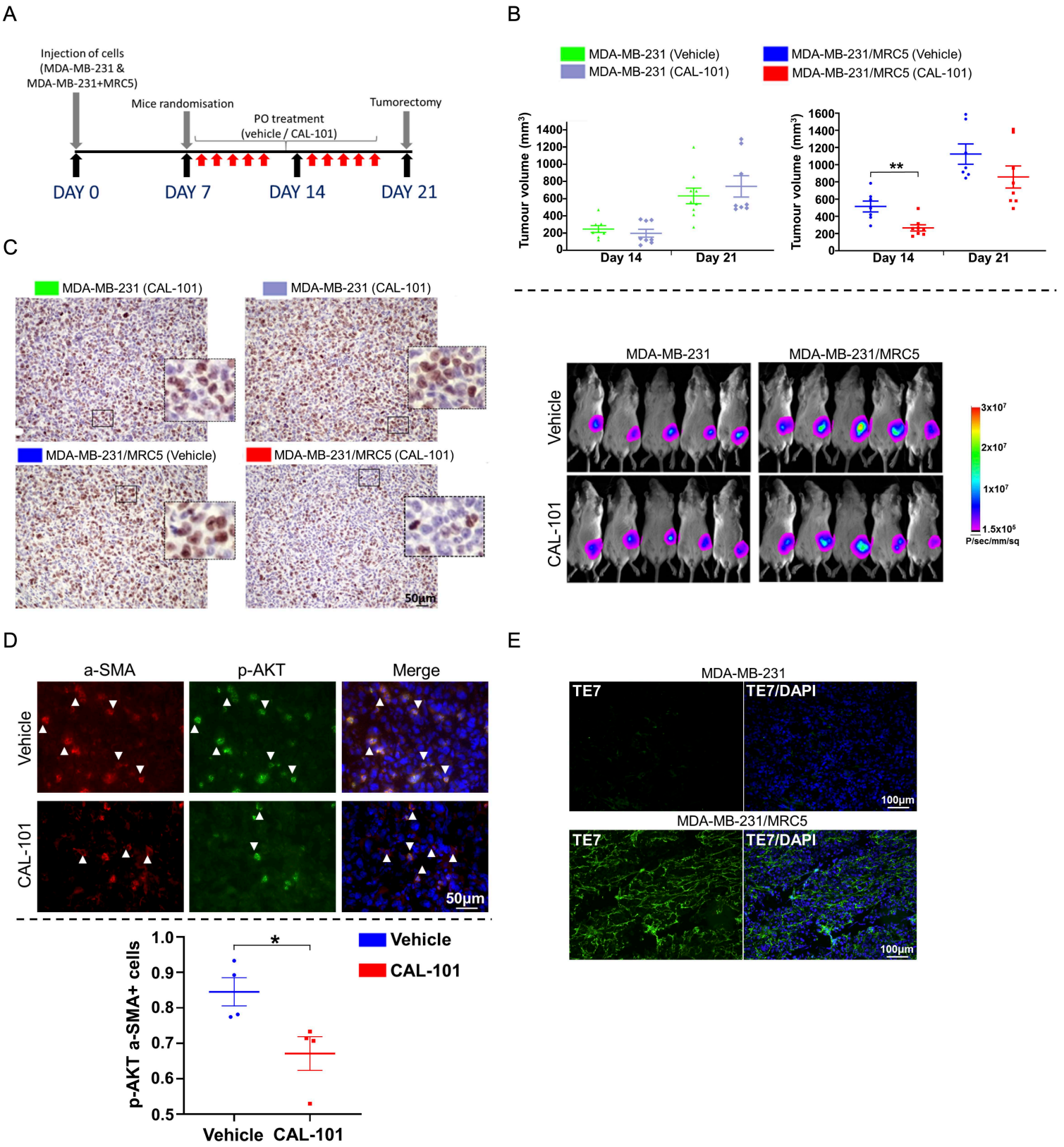
A
Injection of cells (MDA-MB-231 & MDA-MB-231+MRC5)
Mice randomisation
PO treatment (vehicle / CAL-101)
Tumorectomy
DAY 0
DAY 7
DAY 14
DAY 21
B
MDA-MB-231 (Vehicle)
MDA-MB-231 (CAL-101)
MDA-MB-231/MRC5 (Vehicle)
MDA-MB-231/MRC5 (CAL-101)
Tumour volume (mm³)
Day 14
Day 21
**
C
MDA-MB-231 (CAL-101)
MDA-MB-231 (CAL-101)
MDA-MB-231/MRC5 (Vehicle)
MDA-MB-231/MRC5 (CAL-101)
50µm
MDA-MB-231
MDA-MB-231/MRC5
Vehicle
CAL-101
3x10⁷
2x10⁷
1x10⁷
1.5x10⁵
P/sec/mm/sq
D
a-SMA
p-AKT
Merge
Vehicle
CAL-101
50µm
p-AKT a-SMA+ cells
*
Vehicle
CAL-101
E
MDA-MB-231
TE7
TE7/DAPI
100µm
MDA-MB-231/MRC5
TE7
TE7/DAPI
100µm

Figure 7: Effects of fibroblast-PIK3Cδ inhibition on TNBC tumor growth *in vivo*.

(**A**) Schematic representation of the *in vivo* experiment using NOD CB17 PRKDC/J mice. MDA-MB-231 (Groups 1-2) and MDA-MB-231/MRC5 (Groups 3-4) tumor cells were implanted s.c. on day 0. After randomization on day 7, treatment with CAL-101 was initiated in Groups 2 and 4, whereas Groups 1 and 3 were administrated with vehicle. During the course of the study, the growth of the subcutaneously implanted primary tumors was determined twice weekly by luminescence and caliper measurement. (**B**) Upper panel: Box and whisker plots comparing different groups at Day14 and Day 21. Significance was calculated using unpaired t-test. Results are expressed as mean ± SEM; ** $P < 0.01$. Lower panel: Representative *in vivo* images of different groups, treated with vehicle or CAL-101. (**D**) Histological analysis of Ki67 expression in representative tumor tissue sections of different groups. Original magnification, 20×. (**D**) Representative images of immunofluorescent staining of MDA-MB-231/MRC5 tumor cryosections for α-SMA and p-AKT^{Ser473} after DMSO or CAL-101 treatment. Significance was calculated using unpaired t-test. Results are expressed as mean ± SEM; * $P < 0.05$ vs vehicle treated tumors. Original magnification, 40×.(**E**) Representative images of immunofluorescence staining of tumor cryosections using TE-7 anti-human fibroblast antibody. Original magnification, 20×.

Figure 8

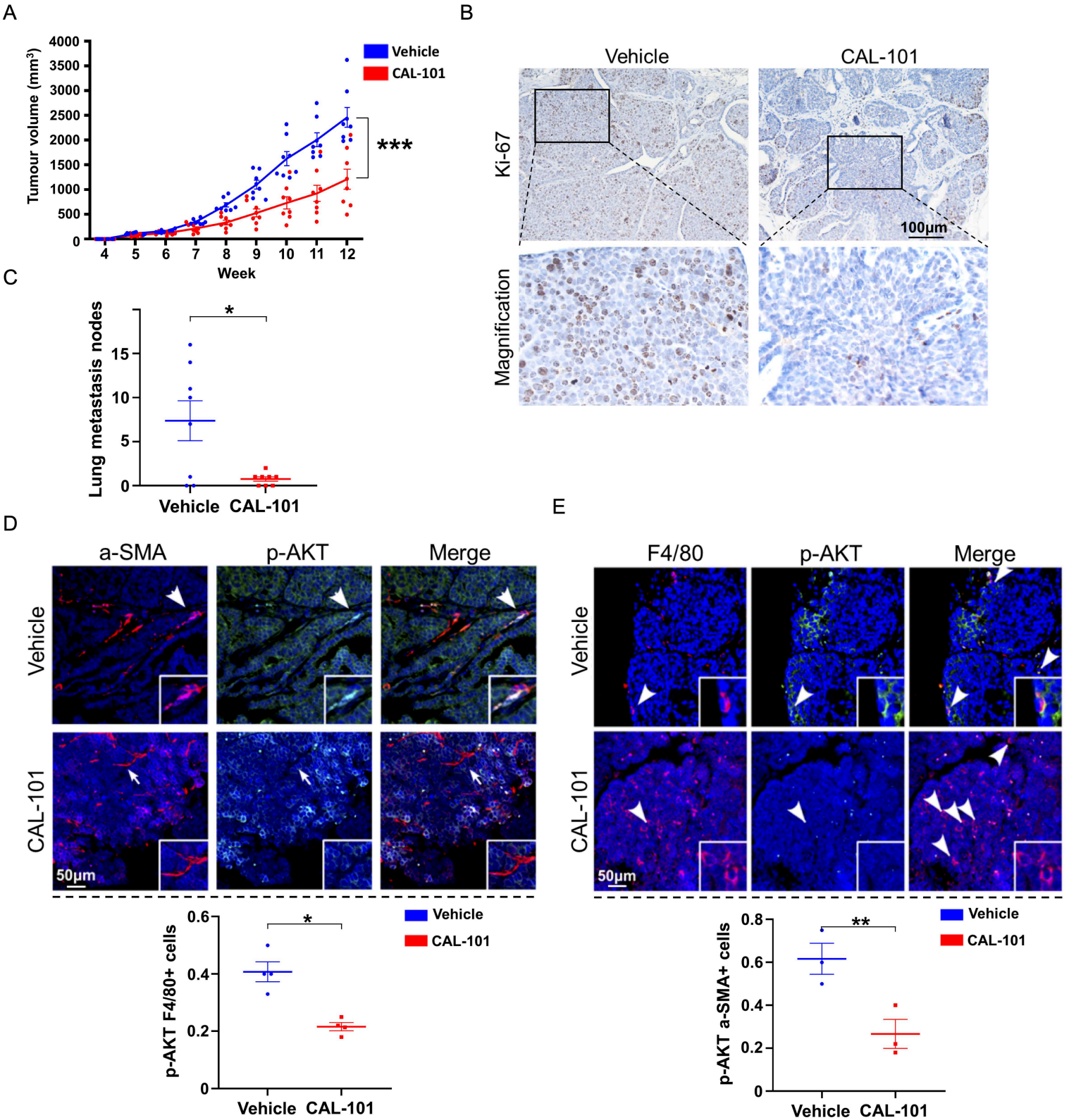
A
Tumour volume (mm³)
4000
3500
3000
2500
2000
1500
1000
500
0
4 5 6 7 8 9 10 11 12
Week
Vehicle
CAL-101
***
B
Vehicle
CAL-101
Ki-67
Magnification
100μm
C
Lung metastasis nodes
15
10
5
0
*
Vehicle CAL-101
D
a-SMA
p-AKT
Merge
Vehicle
CAL-101
50μm
p-AKT F4/80+ cells
0.6
0.4
0.2
0
*
Vehicle
CAL-101
Vehicle CAL-101
E
F4/80
p-AKT
Merge
Vehicle
CAL-101
50μm
p-AKT a-SMA+ cells
0.8
0.6
0.4
0.2
0
**
Vehicle
CAL-101
Vehicle CAL-101

Figure 8: Effects of CAL-101 treatment on tumor growth of MMTV-PyMT transgenic mice.

(**A**) Tumor volumes chart from MMTV-PyMT transgenic mice after vehicle or CAL-101 treatment (n=8 mice / group). Individual values for each mouse are displayed. Significance was calculated using unpaired t-test (week 12). Results are expressed as mean ± SEM; *** $P < 0.001$. **(B)** Representative images for immunohistochemical Ki-67 staining in the mammary tumor sections of MMTV-PyMT transgenic mice after vehicle or CAL-101 treatment. **(C)** Quantification of lung metastatic nodules in each group. Significance was calculated using unpaired t-test. Results are expressed as mean ± SEM; * $P < 0.05$. Yellow and black dots represent mice that were sacrificed at week 12 or week 15 respectively. **(D)** Left panel: Representative images of immunofluorescent staining for α-SMA and p-AKT^{Thr308} in the mammary tumor sections of MMTV-PyMT transgenic mice after vehicle or CAL-101 treatment. Arrows indicate a-SMA^{+} fibroblasts. Higher-magnification images are shown at the bottom right corner. Right panel: Quantification of p-AKT^{Thr308} immunofluorescent staining in tumor infiltrating a-SMA^{+} fibroblasts in the mammary tumors of MMTV-PyMT transgenic mice after vehicle or CAL-101 treatment. Significance was calculated using multiple t-tests. Results are expressed as mean ± SEM; ** $P < 0.01$ vs. vehicle treated tumors. (**E**) Left panel: Representative images of immunofluorescent staining for F4/80 and pAKT^{Thr308} in the mammary tumor sections of MMTV-PyMT transgenic mice after vehicle or CAL-101 treatment. Arrows indicate F4/80^{+} macrophages. Higher-magnification images are shown at the bottom right corner. Right panel: Quantification of pAKT^{Thr308} immunofluorescent staining in tumor infiltrating F4/80^{+} macrophages in the mammary tumors of MMTV-PyMT transgenic mice after vehicle or CAL-101 treatment. Significance was calculated using multiple t-tests. Results are expressed as mean ± SEM; * $P < 0.05$ vs vehicle treated tumors.

Figure 9

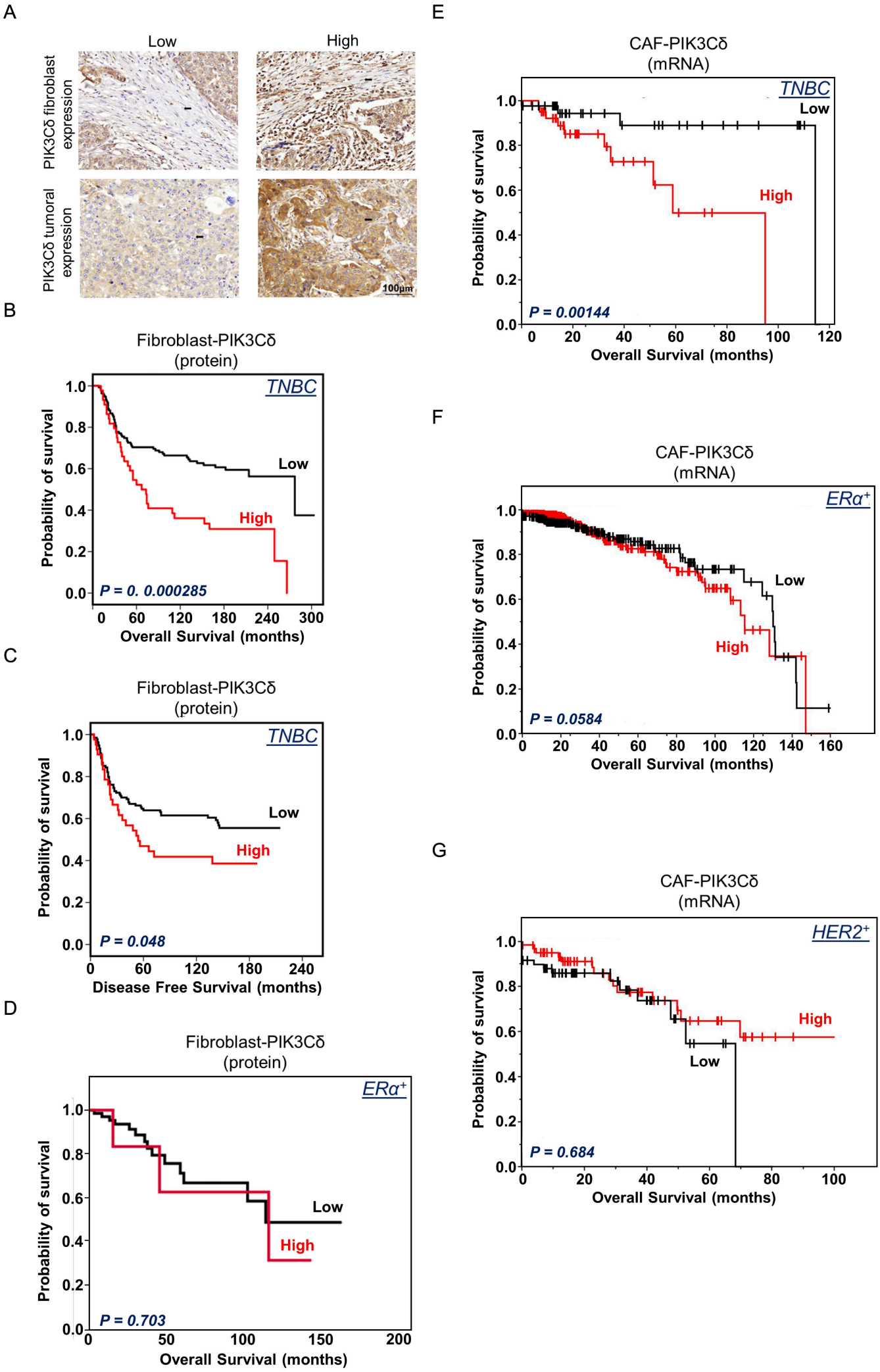
A
Low
High
PIK3Cδ fibroblast expression
PIK3Cδ tumoral expression
100µm
B
Fibroblast-PIK3Cδ (protein)
TNBC
Low
High
P = 0. 0.000285
Probability of survival
Overall Survival (months)
C
Fibroblast-PIK3Cδ (protein)
TNBC
Low
High
P = 0.048
Probability of survival
Disease Free Survival (months)
D
Fibroblast-PIK3Cδ (protein)
ERα+
Low
High
P = 0.703
Probability of survival
Overall Survival (months)
E
CAF-PIK3Cδ (mRNA)
TNBC
Low
High
P = 0.00144
Probability of survival
Overall Survival (months)
F
CAF-PIK3Cδ (mRNA)
ERα+
Low
High
P = 0.0584
Probability of survival
Overall Survival (months)
G
CAF-PIK3Cδ (mRNA)
HER2+
High
Low
P = 0.684
Probability of survival
Overall Survival (months)

Figure 9: PIK3Cδ expression in fibroblast cells and association with patients' survival. (**A**) Representative images of low and high PIK3Cδ expression in tumor or surrounding fibroblast cells (a-SMA^{+}). Original magnification ×20. (**B**) Kaplan-Meier plots showing the association between fibroblast-PIK3Cδ protein expression with OS (Log rank test; P = 0.000285) in TNBC patients. (**C**) Kaplan-Meier plots showing the association between fibroblast-PIK3Cδ protein expression with DFS (Log rank test; P = 0.048) in TNBC patients. (**D**) Kaplan-Meier plots showing the association between fibroblast-PIK3Cδ protein expression with OS (Log rank test; P = 0.703) in ERα^{+}patients. (**E**) Kaplan-Meier plots showing the association between CAF-PIK3Cδ mRNA expression with OS (Log rank test; P = 0.001) in TNBC patients following deconvolution of bulk TCGA RNA-seq samples. (**F**) Kaplan-Meier plots showing the association between CAF-PIK3Cδ mRNA expression with OS (Log rank test; P = 0.058) in ERα^{+} patients following deconvolution of bulk TCGA RNA-seq samples. (**G**) Kaplan-Meier plots showing the association between CAF-PIK3Cδ mRNA expression with OS (Log rank test; P = 0.684) in HER2^{+} patients following deconvolution of bulk TCGA RNA-seq samples.